CHARACTERIZING LOSSES IN MICROSTRIP TRANSMISSION LINES

by

Rashmi Pathak

A dissertation submitted in partial fulfillment of
the requirements for the degree of

Master of Science

(Electrical and Computer Engineering)

at the

UNIVERSITY OF WISCONSIN–MADISON

Summer 2005

Characterizing Losses in Transmission Lines

Rashmi Pathak

Under the supervision of Professor Peter Timbie and Professor Daniel van der Weide

ACKNOWLEDGMENTS

First of all I would like to thank my advisors Prof. Daniel van der Weide and Prof. Peter Timbie for their unlimited devotion, support and advice during my work. The comfort level that they created while working with me motivated me to perform at my best. Also thanks to my lab-mates, Siddharth Malu and Shafinaz Ali, who contributed useful feedback throughout the course of this research, helping me back on track whenever I derailed. Siddharth also looked closely at the final version of the thesis and offering suggestions for improvement.

I would like to express my gratitude to all those who gave me the possibility to complete this thesis. In exception of my work effort, there have been several people contributing to the quality of this study.

Finally a special thanks to my parents and elder sister for giving me immense strength not only to set high goals but also to achieve them. Without their support, this effort would not have been possible.

DISCARD THIS PAGE

TABLE OF CONTENTS

Page

DISCARD THIS PAGE

LIST OF FIGURES

Appendix
Figure Page

Appendix
Figure

DISCARD THIS PAGE

LIST OF TABLES

ABSTRACT

The final goal of this work is to study the losses involved in superconducting microstrip transmission lines in the W-band in a cryogenic setup. A scale model with finite conductivity material is built to work in the X-band. The microstrip is fed by slots in the ground plane which are in turn fed by waveguides. The transmission parameter for various lengths of lines is measured and compared to the experimental setup. The microstrip lines are de-embedded from the waveguide-to-slot and slot-to-microstrip transitions present. Extensive simulations are also carried out to provide insight into the results obtained from the experiments. Different parameters like the slot dimensions, microstrip dimensions and the dielectric thickness were tweaked in the simulations to reduce the mismatch between the transitions and facilitate better transmission. The experimental results show a low transmission between the lines which is supported by the simulation results.

Chapter 1

Introduction

Of the various guided wave structures used in the transmission of microwave signals the microstrip line is probably the most popular because of its simple geometry, small size and the ease with which it can be integrated, all very desirable properties in modern technology. In order to be able to design microstrip lines having the desired electrical properties in a given application, certain electrical parameters, namely the distributed resistance, inductance, conductance and capacitance, must be known. The use of superconductors in constructing microstrip lines results in a negligibly small distributed resistance, which is the main cause of losses when using normal conductors.

Making high quality measurements of the millimeter-wave properties of superconducting thin-film microstrip transmission lines has been studied in the literature. In particular, Vayonakis et al. [13] have developed an *on-chip* technique based on standing wave resonances in an open ended Nb/SiO/Nb microstrip stub. Millimeter-wave radiation is coupled onto the chip fabricated on a thick silicon substrate. Two Nb/Al-oxide/Nb SIS junctions on the chip serve as direct detectors. One of the junctions is connected to an open-ended Nb/SiO/Nb microstrip stub. The ratio of the signal from the junction connected to the stub, to the signal from the power reference junction, gives a precise relative power response, whose frequency dependence carries information about the properties of the microstrip stub. They conclude that the loss is dominated by the SiO dielectric.

In this work we are building similar superconducting structures but without the cryogenic detectors. The assembly is simple and allows rapid comparisons of microstrip designs

by repositioning of the waveguide sections on the slot/microstrip. The superconducting microstrip lines are to be used in a cryogenic setup in a cryostat cooled to less than 4.2 K. We are using superconducting lines in order to minimize losses. Our first goal is to measure the loss per unit length of superconducting microstrip lines. Later we plan to study various superconducting microstrip structures, such as filters, hybrid couplers, etc. Multiple lines of different lengths are fed by slots in the ground plane. Microstrips are coupled to these slots which are fed by straight waveguide sections. Previous studies of waveguide to microstrip transitions involved modification of the waveguide with E-plane probe-transitions [5] and ridged waveguide-transitions [10]. Simon et al. [12] talks about a coplanar transmission line to rectangular waveguide transition without the modifications in the waveguide with the possibility of hermetic sealing. Kooi et al. [9] describes a waveguide to thin-film microstrip transition for high-performance sub-millimeter wave and terahertz applications. A Broadband Microstrip-to-Waveguide Transition Using Quasi-Yagi Antenna is presented in Kaneda et al. [7]. All these approaches require embedding the microstrip and microstrip-to-waveguide transition in a waveguide block. In a cryogenic setting, this arrangement allows only one device to be tested per cooldown of the dewar, unless the cryostat is outfitted with multiple waveguides. Tests of multiple devices would be very time consuming. Instead, we wish to develop a microstrip-to-waveguide transition that can be repositioned inside a cryostat at low temperature. It is not necessary to optimize transition impedance mismatches in order to characterize microstrip parameters. Losses in different lengths of microstrips are measured using this assembly making it possible to characterize and normalize out the transitions through de-embedding. The measurements are made on a scale model at X-band (6-12 GHz). Microwaves are sent through a waveguide and coupled into one end of the microstrip and detected at the other end. The ratio of the output to input power of different lengths of transmission lines is measured. The actual measurements would be made in a cryogenic setup at W-band frequencies (75-110 GHz). The microstrip transmission lines would be superconducting at the higher frequencies.

Chapter 2

Background

2.1 Transmission Lines

An isotropic or omnidirectional electromagnetic source radiates waves equally in all directions. Even when the source radiates through a highly directive antenna, its energy spreads over a wide area at large distances. This radiated energy is not guided, and the transmission of power and information from the source to a receiver is inefficient. For efficient point-to-point transmission of power and information the source energy must be directed or guided. This can be achieved by using transmission lines. A transmission line is no more than a physical connection between two locations through two conductors. Any transmission of energy through conducting or nonconducting media may be considered a transmission line. Also, any guiding of energy by physical structures may be included in this general definition. Examples of transmission lines include parallel conducting wires such as overhead power transmission lines made of thick cables and suspended from towers. Another common type of transmission line is the coaxial transmission line which is made of two coaxial conductors: an inner, thin, solid conductor and an outer hollow cylindrical conductor. The latter is usually stranded to allow more flexibility and the two conductors are insulated with some dielectric material. Another type of transmission line is the parallel plate transmission line also called the stripline. This line consists of two parallel conducting plates separated by a dielectric slab of a uniform thickness, such as strips on printed circuit boards.

A transmission line is usually characterized by three types of parameters:

1. Dimensional parameters: These include length, dimensions of each conductor (thickness, width, diameter etc), spacing between lines, thickness of insulation, etc. These parameters define the physical configuration of the line but also play a role in defining its electrical properties.

2. Material parameters: The line is made of conductors and insulators. The electrical properties of these materials are their conductivities, permittivity, and permeability. These obviously affect the way a line performs its task.

3. Electrical parameters: These are the resistance (R), capacitance (C), inductance (L), and conductance (G) per unit length of the line. R is due to the finite conductivity of the metal conductors, C is due to the separation of two metal plates with a dielectric, L is due to the inductance of the conductors and G is due to the dielectric loss.

When a wave is driven down a transmission line of infinite length there is no power loss due to reflection since the line is infinite. To obtain complete transmission for a finite length of transmission line the line needs to be terminated by an impedance known as the characteristic impedance (Z_0). If a load equal to the characteristic impedance is placed at the output end of any length of line, the same impedance will appear at the input terminals of the line. Characteristic impedance is entirely different from leakage resistance of the dielectric separating the two conductors, and the metallic resistance of the wires themselves. It is a function of the capacitance, inductance, resistance and conductance distributed along the line's length, and would exist even if the dielectric were perfect (infinite conductance) and the wires superconducting (zero resistance).

2.1.1 Microstrips

A microstrip line is, by definition, a transmission line consisting of a strip conductor and a ground plane separated by a dielectric medium. Fig. 2.1 illustrates the microstrip geometry. The dielectric material serves as a substrate and is sandwiched between the strip conductor and the ground plane. Some typical dielectric substrates are RT/Duroid (a trademark of

Rogers corporation, Chandler, Arizona), which is available with several values of ϵ_r (e.g., $\epsilon = 2.23\epsilon_r$, $\epsilon = 6\epsilon_r$, $\epsilon = 10.5\epsilon_r$, etc.); quartz ($\epsilon = 3.7\epsilon_r$), alumina ($\epsilon = 9\epsilon_r$).

The electromagnetic field lines in the microstrip are not contained entirely in the substrate. If one solves the electromagnetic equations to find the field distributions, one finds very nearly a completely TEM (transverse electromagnetic) pattern. This means that there are only a few regions in which there is a component of electric or magnetic field in the direction of wave propagation. Fig. 2.2 illustrates the quasi-TEM behavior of microstrip lines. Assuming a quasi-TEM mode of propagation in the microstrip line, the phase velocity is given by

$$v_p = \frac{c}{\sqrt{\epsilon_{eff}}} \tag{2.1}$$

where c is the speed of light (i.e., 3×10^8 m/s) and ϵ_{eff} is the relative dielectric constant of the microstrip. The effective relative dielectric constant of the microstrip is related to the dielectric constant of the dielectric substrate and also takes into account the effect of the external electromagnetic fields (i.e., fringing effects must be considered).

Since

$$Z_0 = \sqrt{\frac{L}{C}} \tag{2.2}$$

and

$$v_p = \frac{1}{\sqrt{LC}} \tag{2.3}$$

the characteristic impedance of the microstrip line can be expressed in the form

$$Z_0 = \frac{1}{v_p C} \tag{2.4}$$

The wavelength in the microstrip is given by

$$\lambda = \frac{v_p}{f} = \frac{c}{f\sqrt{\epsilon_{eff}}} = \frac{\lambda_0}{\sqrt{\epsilon_{eff}}} \tag{2.5}$$

where λ_0 is the freespace wavelength.

It is good to have a high dielectric constant substrate and a slow wave propagation velocity; this reduces the radiation loss from the circuits. However at the higher frequencies

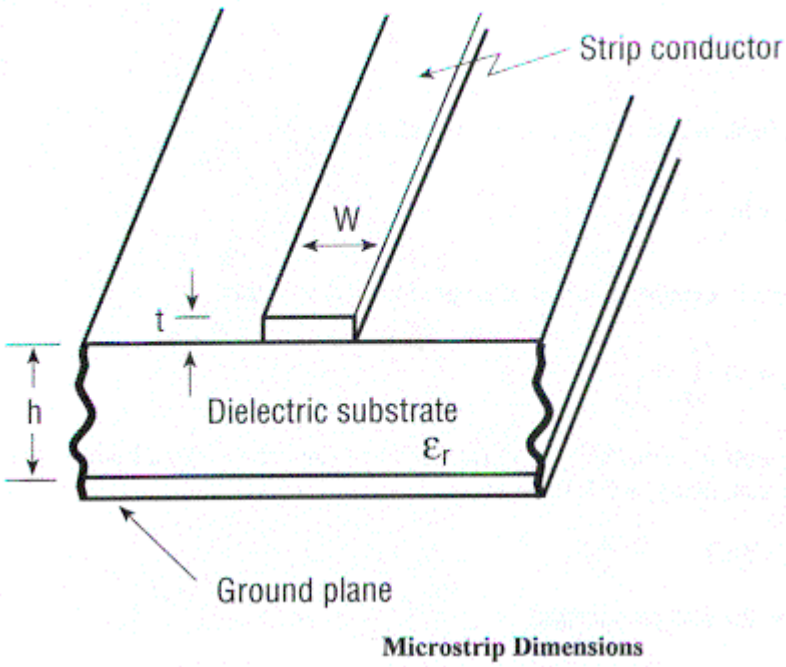

Figure 2.1 Microstrip cross section.

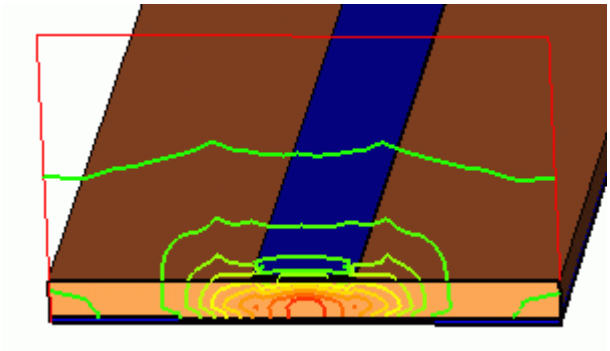

Figure 2.2 Quasi-TEM field configuration

the circuits get impossibly small, which restricts the power handling capability. For these applications one often chooses fused quartz (dielectric constant 3.8).

A microstrip is also characterized by its attenuation. The attenuation constant is a function of the microstrip geometry, the electrical properties of the dielectric substrate and the conductors, and the frequency. There are two types of losses in a microstrip line: a dielectric substrate loss and the ohmic skin loss in the conductors. The losses can be expressed as a loss per unit length along the microstrip line in terms of the attenuation factor α. In dielectric substrates, the dielectric losses are normally smaller than conductor losses. However, dielectric losses in silicon substrates can be of the same order or larger than conductor losses. Microstrips also have radiation losses.

2.2 Slot Antennas

The slot antenna consists of a radiator formed by cutting a narrow slot in a large metal surface. Such an antenna is shown in Fig. 2.3. The slot length is a half wavelength at the desired frequency and the width is a small fraction of a wavelength. This is the first resonance of the slot. The slot has a high impedance at it's first resonance. The antenna is frequently compared to a conventional half-wave dipole consisting of two flat metal strips. The physical dimensions of the metal strips are such that they would just fit into the slot cut out of the large metal sheet. This type of antenna is called the Complementary Dipole. The slot antenna is compared to its complementary dipole to illustrate that the radiation patterns produced by a slot antenna cut into an infinitely large metal sheet and that of the complementary dipole antenna are the same. The slot antenna has a lower impedance at it's second resonance. The length of the slot is twice the wavelength at second resonance.

Several important differences exist between the slot antenna and its complementary antenna. First, the electric and magnetic fields are interchanged. The electric field lines are built up across the narrow dimensions of the slot. As a result, the polarization of the radiation produced by a horizontal slot is vertical. If a vertical slot is used, the polarization is horizontal. In the case of a horizontal dipole antenna the electric lines are horizontal while

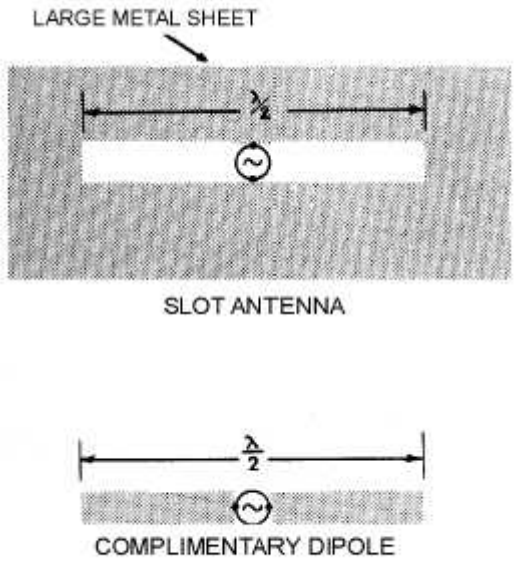

Figure 2.3 Slot Antenna designed to operate at *first resonance*

the magnetic lines form loops in the vertical plane. For these reasons the slot is sometimes described as a "magnetic dipole".

A second difference between the slot antenna and its complementary dipole is that the direction of the lines of electric and magnetic force abruptly reverse from one side of the metal sheet to the other. In the case of the dipole, the electric lines have the same general direction while the magnetic lines form continuous closed loops.

When energy is applied to the slot antenna, currents flow in the metal sheet. These currents are not confined to the edges of the slot but rather spread out over the sheet. Radiation then takes place from both sides of the sheet. In the case of the complementary dipole, however, the currents are more confined; so a much greater magnitude of current is required to produce a given power output using the dipole antenna.

Whether the slot is directly fed or excited by an incident electric field the voltage is clearly zero at the ends and maximum in the middle. Compare this with a half-wave strip dipole of the same size as the slot and similarly oriented in space. Here the voltage distribution has a minimum at the center and maxima at the ends - the reverse of the slot distribution. Booker [1] first showed the complementary nature of slot and dipole and demonstrated the important relationship:

$$Z_1 Z_2 = \left(\frac{120\pi}{2}\right)^2 \tag{2.6}$$

where Z_1 is the impedance of a dipole and Z_2 of its complementary slot. The sign of a slot reactance is opposite to that of a dipole. This can be appreciated if one half of the slot is considered as a short circuited strip transmission line. Then, for lengths less than $\frac{\lambda}{4}$, the input reactance of each half will be inductive whilst that of the equivalent dipole will be capacitive.

2.3 S-parameters

RF and microwave networks are often characterized using scattering or S-parameters. The S-parameters of a network provide a clear physical interpretation of the transmission and reflection performance of the device. The S-parameters for a two-port network are

defined using the reflected or emanating waves, b1 and b2, as the dependent variables, and the incident waves, a1 and a2, as the independent variables. The general equations for these waves as a function of the S-parameters is shown below:

$$b_1 = S_{11}a_1 + S_{12}a_2 \tag{2.7}$$

$$b_2 = S_{21}a_1 + S_{22}a_2 \tag{2.8}$$

S11 - Forward Reflection Coefficient

S21 - Forward Transmission Coefficient

S12 - Reverse Transmission Coefficient

S22 - Reverse Reflection Coefficient

Using these equations, the individual S-parameters can be determined by taking the ratio of the reflected or transmitted wave to the incident wave with a perfect termination placed at the output.

$$S_{11} = \left.\frac{b_1}{a_1}\right|_{a_2=0} \tag{2.9}$$

$$S_{12} = \left.\frac{b_1}{a_2}\right|_{a_1=0} \tag{2.10}$$

$$S_{21} = \left.\frac{b_2}{a_1}\right|_{a_2=0} \tag{2.11}$$

$$S_{22} = \left.\frac{b_2}{a_2}\right|_{a_1=0} \tag{2.12}$$

$$\mathbf{S} = \begin{bmatrix} S_{11} & S_{12} \\ S_{21} & S_{22} \end{bmatrix} \tag{2.13}$$

These four S-parameters completely define the two-port network characteristics. All modern vector network analyzers can easily the measure the S-parameters of a two-port device.

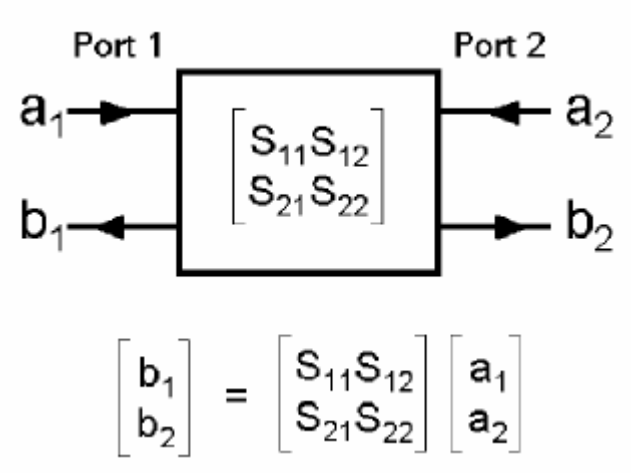

Figure 2.4 Definition of a two-port S-Parameter network.

2.4 T-parameters

Provided that the reflection coefficients S11 and S22 are relatively small, the effect of cascading several two-port networks can be estimated by merely multiplying the S21 coefficients of the individual components (or, if they are in logarithmic units, by adding the dB values of the S21 coefficients). Such a calculation determines, to first order, the magnitude and phase of a signal that propagates straight through the cascade proceeding from left to right through each component. Unfortunately, the overall transfer function of a highly cascaded system equals the product of the S21 terms only when the reflections are negligible. If the reflections are significant, the gain does not equal the product of S21 terms. If the reflections need to be modeled, a more sophisticated analysis is required. That is the purpose of the transmission matrix, also called the Transfer Matrix, or T-parameters. To determine the T-parameters of a two-port network, the incident and reflected waves must be arranged so the dependent waves are related to Port 1 of the network and the independent waves are a function of Port 2. This definition is useful when cascading a series of two-port networks in which the output waves of one network are identical to the input waves of the next. This allows simple matrix multiplication to be used with the characteristic blocks of two-port networks. The T-parameters can be multiplied in case of cascaded networks to determine the T-parameters of the entire network. S-parameters can't be multiplied and hence T parameters are very useful in determining the overall matrix parameters of a cascaded network. The mathematical relationship between the T-parameters and S-parameters is shown below in Figure .

$$\mathbf{T} = \begin{bmatrix} T_{11} & T_{12} \\ T_{21} & T_{22} \end{bmatrix} \tag{2.14}$$

2.5 De-embedding

In many S-parameter measurements, one would desire to make the measurement with some other setup than what one has. A frequent need is to remove the effects of a fixture

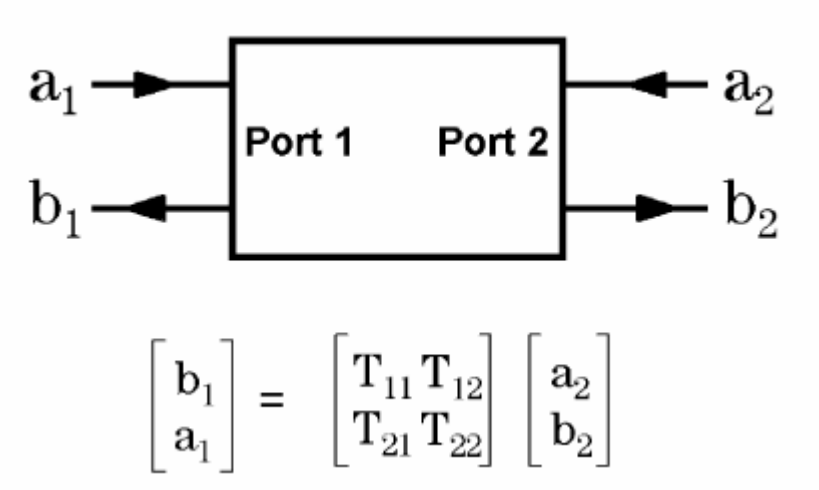

Figure 2.5 Definition of a two-port T-Parameter network.

$$\begin{bmatrix} S_{11} & S_{12} \\ S_{21} & S_{22} \end{bmatrix} = \begin{bmatrix} \frac{T_{12}}{T_{22}} & \frac{T_{11}T_{22}-T_{12}T_{21}}{T_{22}} \\ \frac{1}{T_{22}} & -\frac{T_{21}}{T_{22}} \end{bmatrix}$$

$$\begin{bmatrix} T_{11} & T_{12} \\ T_{21} & T_{22} \end{bmatrix} = \begin{bmatrix} -\frac{S_{11}S_{22}-S_{12}S_{21}}{S_{21}} & \frac{S_{11}}{S_{21}} \\ -\frac{S_{22}}{S_{21}} & \frac{1}{S_{21}} \end{bmatrix}$$

Figure 2.6 Relationship between the S-parameters and T-parameters.

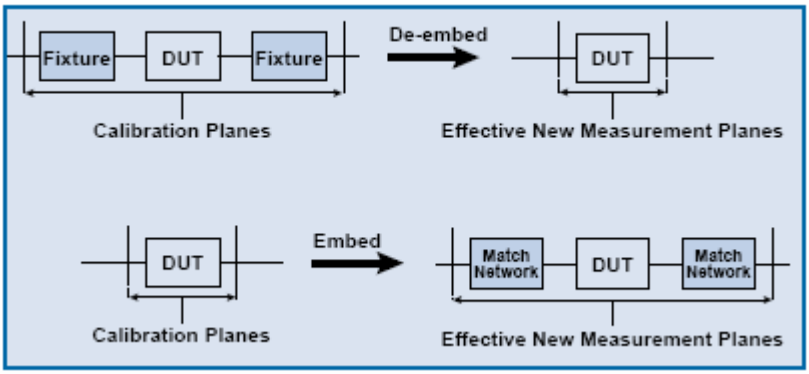

Figure 2.7 De-embedding: Subtracting networks from a measurement.

or virtually add in the effects of other networks (e.g., matching). De-embedding is a tool for virtually subtracting networks to/from measured data on 2,3 or 4 port devices [3]. It uses a model of the fixture and mathematically removes the fixture characteristics from the overall measurement. This fixture "de-embedding" procedure can produce very accurate results for the non-coaxial device-under-test (DUT), without complex non-coaxial calibration standards. The process of de-embedding a test fixture from the DUT measurement can be performed using scattering transfer parameters (T-parameter) matrices. The de-embedded measurements can be post-processed from the measurements made on the test fixture and DUT together.

The classical de-embedding problem is the removal of the effects of a fixture. If one can treat the fixture/probe as a simple length of 50 ohm transmission line, then the problem reduces to one of shifting the reference planes. To determine how much the planes should be moved, the distance can be physically measured. Also, shorts or opens can be placed at the actual DUT planes and an "auto reference plane" extension function can be used to calculate the distance required to put the reference plane exactly where the DUT was placed. If the fixture is more complicated then this simple model of the fixture as a pure 50 ohm transmission line may be unacceptable. This is where more complete de-embedding is used to mathematically remove the fixture effects. The fixture must be characterized before it can

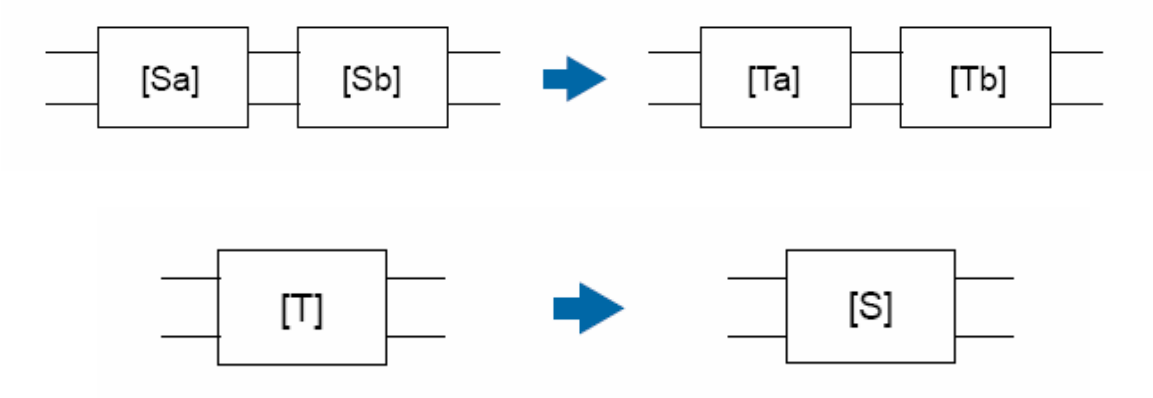

Figure 2.8 S parameter calculation of cascaded networks.

be removed from the data. Before the mathematical process of de-embedding is developed, the test fixture and the DUT must be represented in a convenient form. Using signal flow graphs, the fixture and device can be represented as three separate two-port networks. In this way, the test fixture is divided in half to represent the coaxial to non-coaxial interfaces on each side of the DUT. The two fixture halves will be designated as Fixture A and Fixture B for the leftward and right-hand sides of the fixture respectively. The S-parameters FAxx (xx = 11, 21, 12, 22) will be used to represent the S-parameters for the left half of the test fixture and FBxx will be used to represent the right half.

Because we defined the test fixture and DUT as three cascaded networks, we can easily multiply their respective T-parameter networks, TA, TDUT and TB.

This matrix operation will represent the T-parameters of the test fixture and DUT when measured by the VNA at the measurement plane. Extending this matrix inversion to the case of the cascaded fixture and DUT matrices, each side of the measured result is multiplied by the inverse T-parameter matrix of the fixture and T-parameter for the DUT is obtained. The T-parameter matrix can then be converted back to the desired S-parameter matrix.

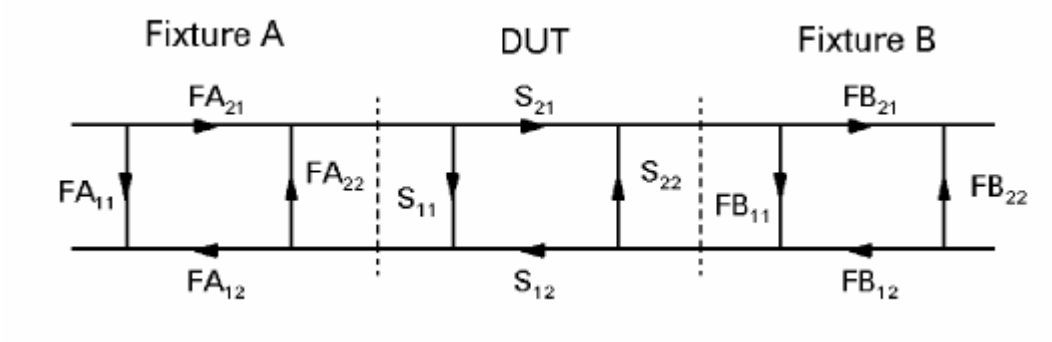

Figure 2.9 Signal flow graph representing the test fixture halves and the DUT

2.6 Software

2.6.1 Computational Modeling

Electromagnetic fields can be predicted by experiment, analysis and computation. The last mentioned technique, otherwise known as numerical simulation, is the most recent and rapidly advancing. Electromagnetic fields, like many other physical processes, are governed by partial differential equations (PDEs). Hence the numerical methods for solving such problems can be classed with other methods of solving PDEs, such as the Finite Element method, Method of Moments and Finite Difference method. Every modeling technique has some strengths and some weaknesses.

Electromagnetic simulators can give very accurate solutions for microwave circuits with ideal conductors. When the conductors are non-ideal, accurate results may still be obtained in many cases by specifying material parameters or surface impedances. However, for structures in which the penetration depth of the field into the conductors is of the same order as the conductor thickness, considerable error can occur. [8] talks about surface impedance of superconductors and normal Conductors in EM Simulators.

2.6.1.1 Finite Element Method (FEM)

The finite element method is one of the most successful *frequency domain* computational methods for electromagnetic simulations. The method's main advantage is its capability

to treat any type of geometry and material inhomogeneity without a need to alter the formulation or the computer code. That is, it provides geometrical fidelity and unrestricted material treatment. A number of commercial finite element analysis packages like Ansoft HFSS, Maxwell 2D, Maxwell 3D, FEMLAB Electromagnetics Module are currently available.

The finite element method belongs to the class of partial differential equation (PDE) methods. It is used for modeling a wide class of problems by breaking up the computational domain (meshing) into elements of simple shapes. By keeping the elements small enough (typically less than 1/10 of a wavelength per side), the field interior to the element can be safely approximated by some linear, or, if necessary, higher order expansion. The collection of these elements and their associated expansion or *shape function* is therefore capable of modeling arbitrary and rather complex fields in terms of unknown coefficients which may represent the field values at the nodes (node-based basis) or the average field values over the edges (edge-based basis). Once the shape functions are chosen, it is possible to program the computer to solve complicated geometries by solely specifying the basis functions. The element choice, however, needs human intervention and intelligence to ensure a reliable solution of the problem at hand. Finite element shape functions have compact support within each element, i.e., their scope of influence is limited only to the immediate neighboring elements. This feature plays a pivotal role in the viability of finite elements over integral equation (IE) methods. The limited scope of influence for the basis functions is a distinguishing property of PDE techniques and leads to very sparse matrices in finite elements, whereas IE techniques give rise to full, dense matrices resulting in poor scalability as problem size increases. Sparse matrices can be stored with low memory requirements when iterative solvers are employed for the solution of these systems.

In order to obtain a unique solution, it is necessary to constrain the values of the field at all boundary nodes. For example, the metal box of a model constrains the tangential electric field at all boundary nodes to be zero. A major weakness of the finite element method is that it is relatively difficult to model open configurations (i.e. configurations where the fields are not known at every point on a closed boundary). Various techniques such as ballooning

and absorbing boundaries are used in practice to overcome this deficiency. These techniques work reasonably well for 2-dimensional problems, but so far they are not very effective for 3-dimensional electromagnetic radiation problems. The major advantage that finite element methods have over other EM modeling techniques stems from the fact that the electrical and geometric properties of each element can be defined independently. This permits the problem to be set up with a large number of small elements in regions of complex geometry and fewer, larger elements in relatively open regions. Thus it is possible to model configurations that have complicated geometries and many arbitrarily shaped dielectric regions in a relatively efficient manner.

2.6.1.2 Method of Moments (MoM)

The basic idea is to reduce a functional equation (operator equation) to a matrix equation and then use a computer to solve the the matrix equation using numerical techniques. The concepts are best expressed in the language of linear spaces (Hilbert spaces) and operators, but we only need a few basics. Moment methods are used extensively throughout the literature in antennas and field based formulations. The method is very general and may be applied to non electromagnetic problems. MoM softwares like Sonnet from Sonnet Software Inc., EMSight from Applied Wave Research Inc., etc. are available commercially. The principle objective is to calculate the primary electromagnetic parameters ie fields, currents etc that are solutions to Maxwell's Equations. The basis for such computer solutions is the classical approximation of a function $f(x)$ using a sum of known basis functions $f_n(x)$

$$f(x) = \sum_n \alpha_n f_n \tag{2.15}$$

The differences between numerical methods are in the electromagnetic quantity being approximated, the expansion function used to approximate the unknown and the strategy employed to determine the coefficients of the expansion.

Consider a general operator equation

$$Lf = g \tag{2.16}$$

where L is an algebraic, an integral or differential operator.
f is the unknown to be determined in E/M problems typically the electric/magnetic current.
g is the excitation or source in E/M typically a plane wave or source driving an antenna.
The unknown f can be expanded in a series of functions f_n

$$f(x) = \sum_n \alpha_n f_n \tag{2.17}$$

Where α_n are unknown constants f_n are known basis functions
Substituting in the operator equation

$$L = \sum_n \alpha_n f_n = g \tag{2.18}$$

Due to linearity of the operator

$$\sum_n \alpha_n L f_n = g \tag{2.19}$$

The basic idea behind MoM is to convert the operator equation $Lf = g$ into a matrix equation and using matrix algebra to solve for an unknown vector α_n. Knowledge of the coefficients α_n now allows f to be found via

$$f = \sum_n \alpha_n f_n. \tag{2.20}$$

2.6.1.3 Finite Difference Time Domain (FDTD) Technique

The Finite Difference Time-Domain (FDTD) is a finite difference method for the solution of electromagnetic problems. It is easy to understand, easy to implement in software, and since it is a *time-domain* technique it can cover a wide frequency range with a single simulation run.

The FDTD method belongs in the general class of differential time domain numerical modeling methods. The method (for the most important general 3D domain) was developed by Yee in 1966. It is derived from the Maxwell's equations that are related to Ampere's

Law and Faraday's Law. These PDEs are replaced by differences in a special way to derive the Yee algorithm. Maxwell's (differential form) equations are simply modified to central-difference equations, discretized, and implemented in software. The equations are solved in a leap-frog manner; that is, the electric field is solved at a given instant in time, then the magnetic field is solved at the next instant in time, and the process is repeated over and over again. When Maxwell's differential form equations are examined, it can be seen that the time derivative of the E field is dependent on the Curl of the H field. This can be simplified to state that the change in the E field (the time derivative) is dependent on the change in the H field across space (the Curl). This results in the basic FDTD equation that the new value of the E field is dependent on the old value of the E field (hence the difference in time) and the difference in the old value of the H field on either side of the E field point in space. Naturally this is a simplified description, which has omitted constants, etc. But the overall effect is as described. The H field is found in the same manner. The new value of the H field is dependent on the old value of the H field (hence the difference in time), and also dependent on the difference in the E field on either side of the H field point. This description holds true for 1-D, 2-D, and 3-D FDTD techniques. When multiple dimensions are considered, the difference in space must be considered in all appropriate dimensions. In order to use FDTD a computational domain must be established. The computational domain is simply the space where the simulation will be performed. The E and H fields will be determined at every point within the computational domain. The material of each cell within the computational domain must be specified. Typically, the material will be either free-space (air), metal (perfect electrical conductors (PEC)), or dielectrics, any material can be used, as long as the permeability, permittivity, and conductivity can be specified. Once the computational domain and the grid material is established, a source is specified. The source can be an impinging plane wave, a current on a wire, or an electric field between metal plates (basically a voltage between the two plates), depending on the type of situation to be modeled. Since the E and H fields are determined directly, the output of the simulation is usually the E or H field at a point or a series of point within the computational domain.

Strengths

FDTD is a very versatile modeling technique. It is a very intuitive technique, so users can easily understand how to use it, and know what to expect from a given model. It allows the user to specify the material at all points within the computational domain. All materials are possible and dielectrics, magnetic materials, etc. can be simply modeled without the need to resort to work arounds or tricks to model these materials.

FDTD is a time domain technique, and when a time-domain pulse (such as a Gaussian pulse) is used as the source pulse, then a wide frequency range is solved with only one simulation. This is extremely useful in applications where resonant frequencies are not known exactly, or anytime that a broadband result is desired.

Since FDTD is a time-domain technique which finds the E/H fields everywhere in the computational domain, it lends itself to providing animation displays (movies) of the E/H field movement throughout the model. This type of display is extremely useful to understanding exactly what is going on in the model, and to help insure that the model is working correctly.

FDTD allows the effects of apertures to be determined directly. Shielding effects can be found, and the fields both inside and outside a structure can be found directly.

FDTD provides the E and H fields directly. Since most EMI/EMC modeling applications are interested in the E/H fields, it is best that no conversions must be made after the simulation has run to get these values.

Since the computational domain must end at some point (or we would be modeling the entire universe!!), a boundary must be established. FDTD has a number of very good absorbing boundary conditions to chose from (and some that are not quite so good). The absorbing boundary condition (ABC) simulates the effect of free space beyond the boundary forever.

Weaknesses

Since FDTD requires that the entire computational domain be gridded, and these grids must be small compared to the smallest wavelength and smaller than the smallest feature

in the model, very large computational domains can be developed, which result in very long solution times. Models with long, thin features, (like wires) are difficult to model in FDTD because of the excessively large computational domain required.

FDTD finds the E/H fields directly everywhere in the computational domain. If the field values at some distance (like 10 meters away) are desired, it is likely that this distance will force the computational domain to be excessively large. Far field extensions are available for FDTD, but require some amount of post processing.

2.6.2 HFSS 9.1 - An FEM code from Ansoft

High Frequency Structure Simulator (HFSS) is a complete solution for modeling arbitrarily shaped, passive 3-D structures. It is a general-purpose tool that can be used for a variety of electromagnetic (EM) modeling applications, including antenna design and analysis, machined-component design and analysis, circuit design and analysis and high-speed digital-circuit design and analysis. We used HFSS extensively for simulations of the microstrip scale model.

2.6.3 Sonnet 9.52

Sonnet Suite is a 3-D MoM Planar High-Frequency Electromagnetic Software, from Sonnet Software Inc. Sonnet Lite is a free feature-limited version of Sonnet's professional Sonnet Suite. Sonnet Lite provides a full-wave EM solution for planar high-frequency designs from 1 MHz through several terahertz. We used this for initial simulations of the microstrip.

2.6.4 SuperMix

"SuperMix" is a software library written to aid in the calculation and optimization of the signal and noise performance of high-frequency circuits, especially those including superconductors and superconducting tunnel junctions [14]. Using this library, C++ programs can

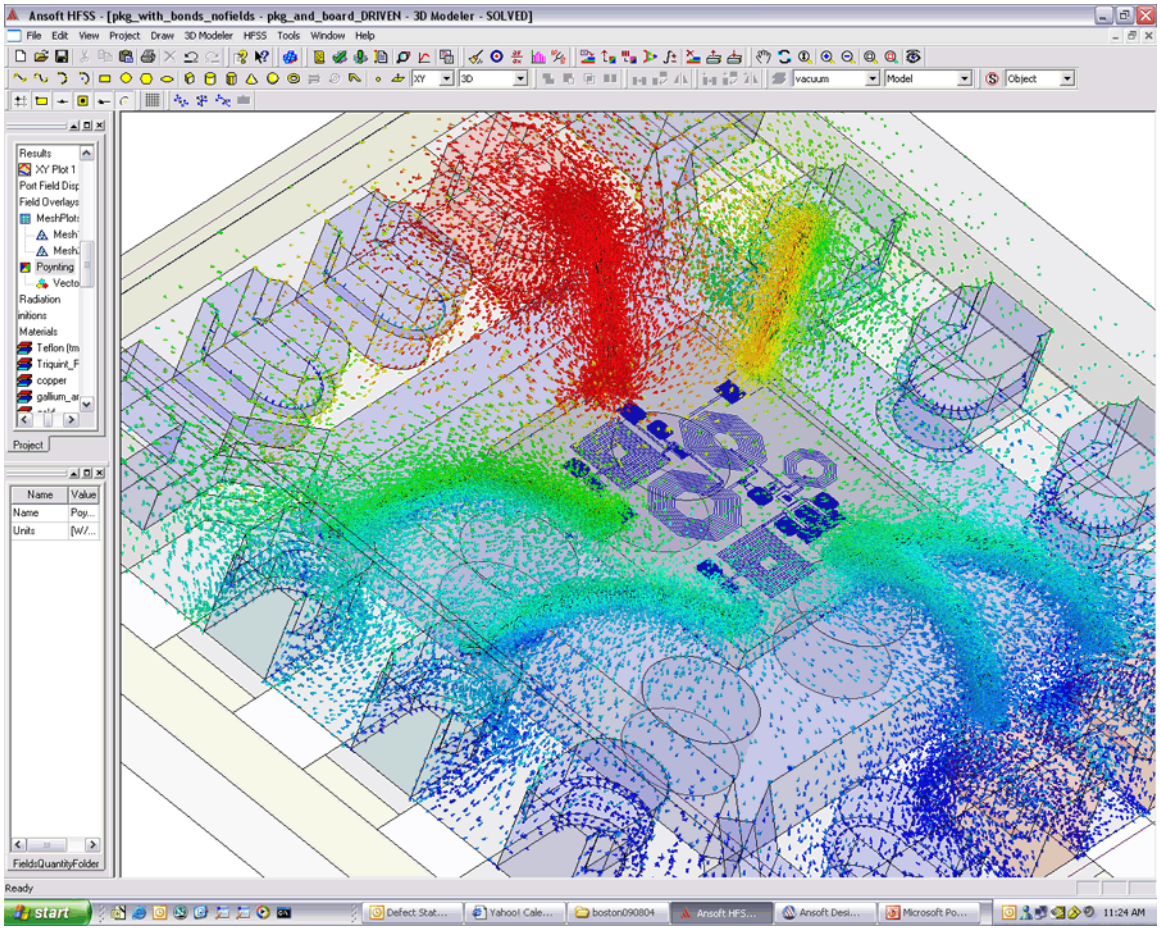

Figure 2.10 GaAs RF Amplifier Package Isolation Analysis using HFSS, showing Power Flow along bondwires

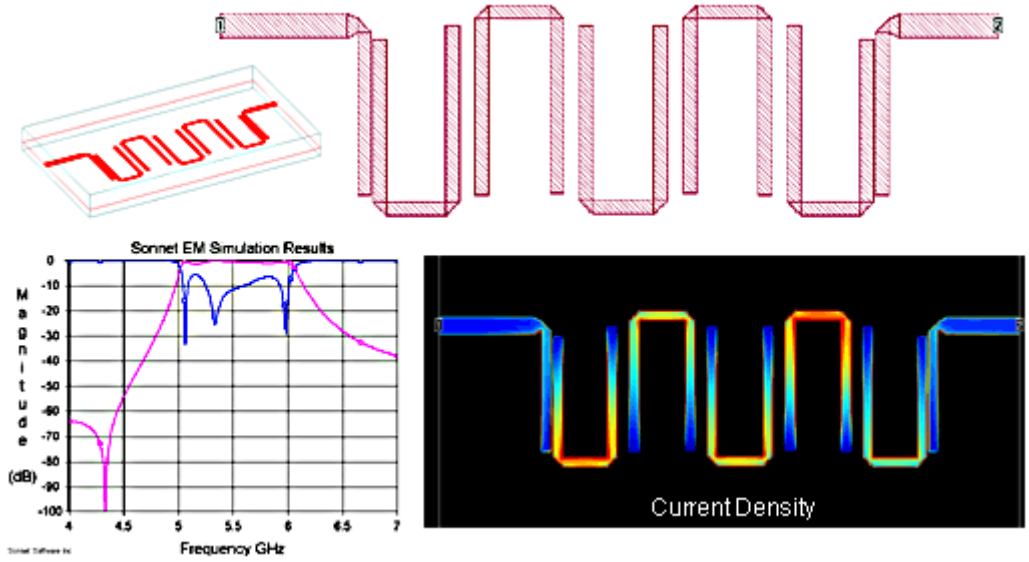

Figure 2.11 Full wave EM solution for a hairpin filter using Sonnet

be written to simulate circuits of arbitrary size, complexity, and topology. The library includes an optimizer which can minimize an arbitrary error function by varying chosen circuit parameters. We used Supermix to calculate the loss/unit wavelength in the W-band.

The SuperMix C++ library includes a number of classes which can be used to calculate the properties of normal and superconducting transmission lines such as the characteristic impedance, and propagation constant. At present, microstrip is the only physical type of transmission line available in SuperMix, although adding new types is straightforward. In particular, the user only needs to calculate the characteristic impedance and the propagation constant; the conversion of these quantities into the scattering matrices is handled by library routines. The characteristics of thin-film transmission lines (such as microstrip) often depend heavily on the surface impedance of the metal conducting films used. At present, SuperMix can calculate the surface impedance for normal metals and superconductors in the case of a local conductivity, defined by Ohm's law. Addition of the nonlocal anomalous skin effect in normal metals is planned for a future release. Multi-layered metal films can also be created. The simplifying assumption is that the conductivity of any given layer is not influenced by the properties of the surrounding layers. This assumption may not be valid in some circumstancesfor instance, in cases where the superconducting proximity effect is important. Transmission lines such as microstrips often use dielectric films or substrates, and the complex dielectric constant of the material must be specified. Dielectrics can be defined in SuperMix by specifying the real part of and the loss tangent,. If necessary, a table of values specifying a frequency-dependent can be read from a data file and automatically interpolated. Actually this can be done for any circuit parameter, and the interpolation can be done with respect to any other parameter (e.g. temperature), not just frequency. Metal films, layered films, and dielectrics form the building-blocks for transmission lines. After the dielectrics and conductors have been specified, transmission lines such as microstrip can be assembled from them.

Chapter 3

Experimental Setup

3.1 Setup

We wanted to build a simple and cheap setup that operated around 10 GHz and scaled 10 times from 100 GHz. The 100GHz experiment would be setup in a cryogenic environment. The setup (Fig. 3.1, Fig. 3.2) was fairly simple and consisted of

3.1.1 FR_4 Board

The FR_4 board is used as a substrate for support. The copper layer on the FR_4 board was 15mm thick. It acted as the ground plane for the microstrip lines.

- Slots: Pairs of slots separated by varying distances were made on the copper ground plane. The slots were 12mm X 1.6mm. The slots were designed for the first resonance.
- Mylar: Mylar is used for the dielectric layer in the microstrip. We used a gauge 10 (0.1mil) thick mylar with an ϵ_r of 3.2.
- Microstrip: A copper wire 3 mils in diameter was used as the microstrip conductor. The line had an impedance of around 10 ohm.
- Waveguide: X-band waveguides were used to feed the slot from the FR_4 side to prevent reflections from the ground plane. Coax-to-waveguide transitions were used to connect the waveguides to the coaxial cables from the VNA.

- Coaxial Cables: Flexible coaxial cables were used. The performance of semi-rigid coaxial cables is affected by the amount of bending and their orientation and in turn affecting the S parameters.
  - The cables should be in good condition.
  - They should operate in the desired frequency band.
  - They should be tested by connecting them together and seeing the bending effects on uncalibrated transmission and reflection measurements.
  - Cables should also be long enough to reach the DUT. It saves a lot of time by checking this before calibrating the VNA with the cables.
  - The connectors should not be tightened excessively. Refer to Appendix B for more information on connectors.
- Eccosorb: Eccosorb was used as an absorbing material for any excess microwaves.
- Clamps: Clamps were used to clamp down the wooden box, with slots to support the waveguide, to the FR4 board. It helped to keep the set-up stable.

3.1.2 VNA

3.1.2.1 Description

Network analysis is the process by which designers and manufacturers measure the electrical performance of the components and circuits used in more complex systems. Vector network analyzers are capable of measuring complex(magnitude and phase) reflection and transmission whereas scalar analyzers can measure only magnitude. network analyzer consists of a sweep oscillator (almost always a synthesizer so that measurements will be repeatable), a test set which includes two ports, a control panel, an information display, and an RF cable or two to hook up your DUT. Each port of the test set includes dual directional couplers and a complex ratio measuring device. Other options include a means for bias

voltage/current injection, and a computer controller to manipulate and store data. Network analyzers can make measurements from 45 MHz to 110 GHz.

3.1.2.2 Calibration

Why? Before jumping into vector network analyzer measurements, the network analyzer needs to be calibrated. Calibration is required to correct for systematic errors in the VNA and cabling. It is necessary to calibrate every time the experiment is newly setup. The experiment was performed using an HP 8720D VNA with a frequency range of 50MHz to 20GHz.

How? There are many types of calibration techniques, and even more types of calibration standards. The reflection calibration for each port requires three standards, typically: an open circuit, a short circuit, and a matched 50-ohm load. The matched load can be a 'broadband load', meaning that it has very low reflection coefficient over a lot of bandwidth. The particular set of cal standards (and test cables) that you use will depend on what frequency band you need to cover. Coaxial calibration kits come in type N, 7 mm, 3.5 mm, 2.92 mm, 2.4 mm, and 1.0 mm. Refer to B.1 for more information on connector handling. Be sure not to exceed the frequency capability of the test set, cables, adapters and calibration kit. A typical calibration will move the measurement reference planes to the very ends of the test cables. You will have the choice of calibrating for reflection or transmission only, using either of the two ports or both of them together. For most tasks you will probably calibrate both test ports for reflection and transmission, which will allow you to measure full two-port scattering matrices (S-parameters for your device under test (DUT).

Validating the calibration: To check the validity of your calibration, as well as the general health of the test equipment, you need to look at a few things after you calibrate. If you are doing transmission measurements, check the residual error in a "through" connection (connect the test cables to each other). You should see 0 dB plus or minus 0.05 dB or better. The phase should be very close to 0.0 degrees as well. The transmission and reflection

parameters should not vary significantly when you gently bend the test cables, or you have a bad connection. If you see a issue with the calibration you just did, figure out the problem before you perform another calibration, or you will be wasting your time and adding needles wear and tear to the cal kit and test cables.

3.2 Photos and Figures

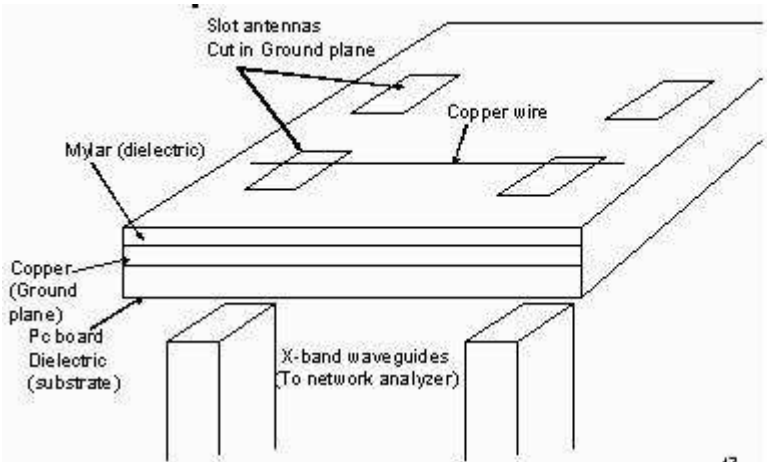

Figure 3.1 Set-up of scale model test. FR_4 PC Board with slots cut in the copper ground plane. Slots feed microstrip with mylar dielectric. X-band waveguides feed slots.

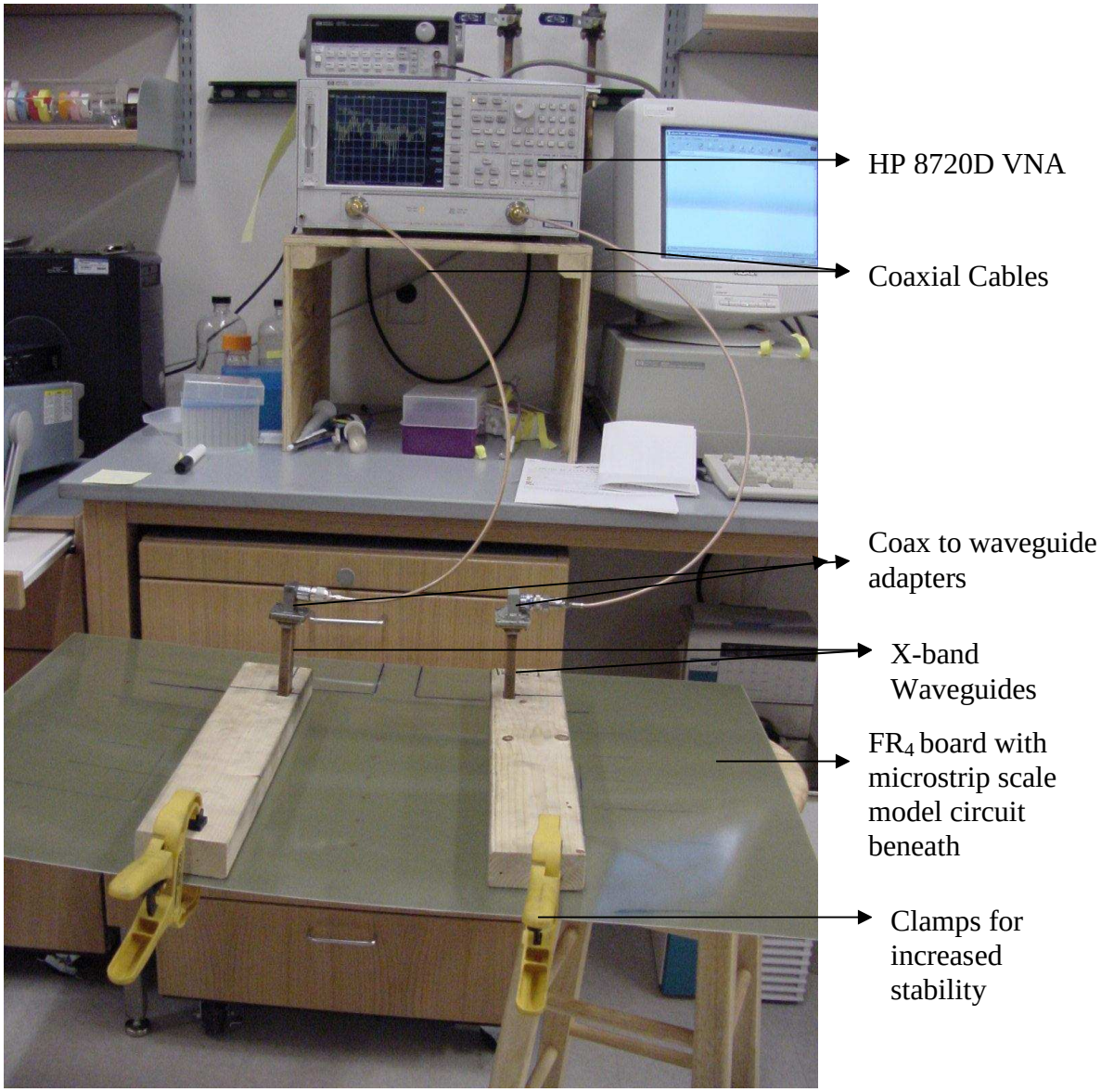

Figure 3.2 Final setup for the scale model test at 10 GHz with the X-band waveguides, slots and a variety of microstrip line lengths.

Chapter 4

Measurements

The real cryogenic tests at 100 GHz with a W-band waveguide require length scales of 3 mm which becomes difficult to fabricate for testing purposes. A variety of scale models (x10) working in X-band, around 8GHz-12GHz, were fabricated and tested. The measurement procedure involved shining microwaves on one end of a transmission line (copper wire) fed by a slot and detecting them at the other end of the line. We started off with a crude scale model but progressed towards a setup almost similar to the cryogenic setup except for the scaled dimensions.

4.1 Scale Model-I

Several different lengths of microstrip transmission lines were fabricated to measure loss *per* wavelength along the frequency band. Some lines were fabricated as straight lines and others as meandering lines. Meanders (Fig.4.1) were used to be able to fabricate different line lengths between two given fixed waveguide locations. Spray-glue was used to attach the mylar, acting as the dielectric, to the FR_4 board and the copper wires to mylar. This resulted in a thickness error within 1 mil.

The signal obtained from the first scale model (Fig. 4.3) was indistinguishable from noise (Fig. 4.2). The amount of power coupled between the waveguides in air was more than the power received through the microstrip. The possible reasons for failure were

- Coupling was not optimized at the waveguide-microstrip transition.
- Waveguide directly placed on the ground plane resulting in a short between the two.

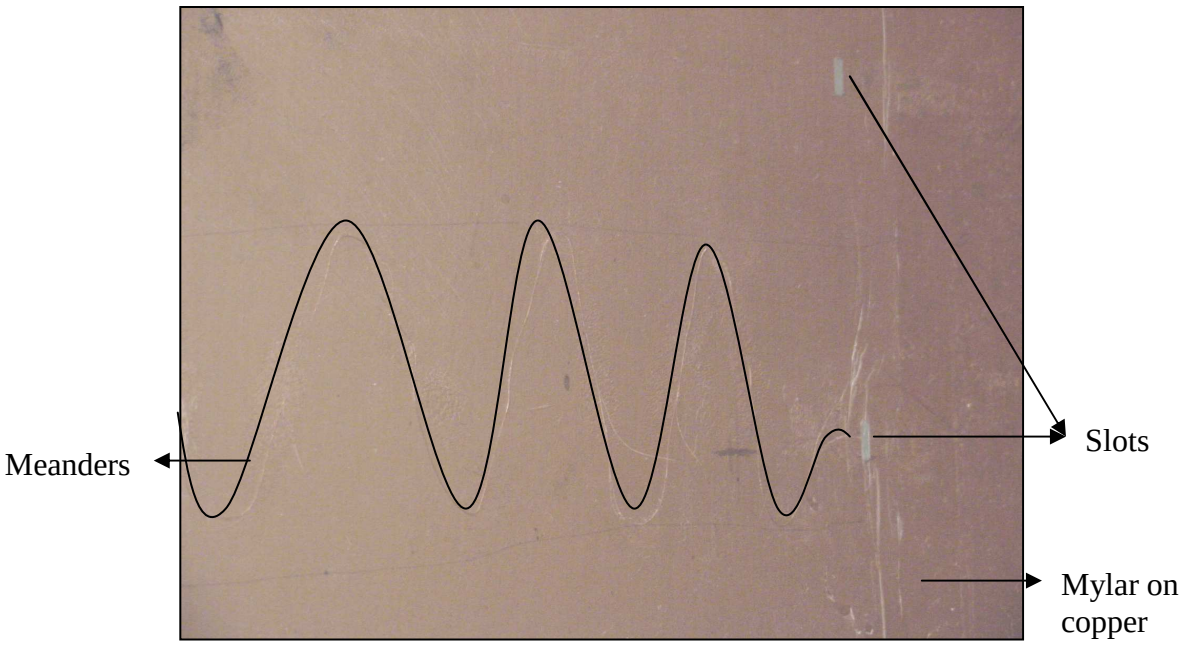

Figure 4.1 Meandering microstrip lines.

- A huge impedance mismatch between the waveguide and the microstrip.

Steps taken to handle the above reasons for failure:

- The waveguide was cut to resonant length to provide a maximum in the electric field at the end of the waveguide.
- The waveguide fed the microstrip lines without shorting with the ground plane. This was accomplished by providing spacers in the setup.

4.2 Scale Model-II

The first scale model did not give a significant amount of signal even after the steps to handle the reasons of failure were incorporated. Some more changes were made in the setup to tackle the problem.

- Due to a high impedance-mismatch a resonant mechanism was required at the waveguide-microstrip transition. A slot in the ground plane was used and the length of the slot

was fixed by the 1^{st} resonant frequency. The width of the slot was chosen to be almost one-tenth of the length.

- The waveguides feeding the slots on the metal side of the FR_4 board resulted in reflective parasitics. Microwaves were shone from the substrate side (Fig. 4.4) of the FR_4 board to reduce the reflections since the FR_4 substrate acts as an anti-reflection coating.

The signal obtained from the microstrip lines was observed to be 15dB greater than the signal obtained from coupling between waveguides in air. The signal was clearly distinguishable and higher than noise. The data obtained were more stable and repeatable. This stability was due to shining microwaves on the substrate side of the FR_4 board. The difference between measurements from lines from different pairs of slots were not significantly different (1dB). Better resonating slots and matching was required.

4.3 Scale Model-III

The waveguide to microstrip transition was tuned further by extending the microstrip by a quarter wavelength beyond the center of the slot. This arrangement ensures a maximum at the center of the slot and thus maximum coupling. The setup was clumsy and time consuming. To improve the consistency and stability of the setup spray-glue was replaced by scotch tape to stick the copper wire onto mylar. Reflection measurements also were taken for consistency check.

The signal obtained by this setup was stable $\pm 1dB$ but was not repeatable. The quality of the SMA connectors affects the signal stability and repeatability.

4.4 Final Scale Model

New SMA connectors and cables were used. The setup was made hands-free to provide more stability and consistency. Waveguide flange was bolted to PC Board for reproducibility. All transitions from coax-to-waveguide, waveguide-to-slot and slot-to-microstrip needed to

be characterized. Only one transition was attempted to be characterized at a time. Measurements on a non-clad substrate board with only slots were taken. Measurements were then taken by adding mylar and microstrip, one at a time. Eccosorb was used to reduce crosstalk. Meanders were too complicated for the initial study of the loss test. The measurements from meanders depend on the number of meanders and the extent of bending. The final setup (Fig. 3.2) involved only straight microstrip lines of different lengths.

All measurements were stable and repeatable. There was a significant difference between different lengths of microstrips. The measurements were still not completely good for high frequencies. Fig. 4.7 shows the raw data obtained directly from the VNA. It shows the transmission parameter (S21) for line lengths of 2", 10", 14" and 18". It clearly shows that the S21 gets worse with increasing line length. The S21 for the 18" line is very noisy. This data includes effects of all the transitions (coax, coax-to-waveguide, waveguide-to-slot, slot-to-microstrip) present.

De-embedding the higher line lengths from the 2" line results in eliminating all the unwanted transition effects. Fig. 4.8 shows the S21 of only the waveguide without the transitions. It shows almost complete transmission through the waveguide, as expected above the cutoff frequency of the X-band waveguide (6.5GHz). Fig. 4.9 shows the various line lengths de-embedded from the 2" line. At frequencies below 10GHz the S21 gets worse with line length. At higher frequencies the results are not good. The reason could be because of the cross coupling between the waveguides for the 2" line which gets dominant at higher frequencies.

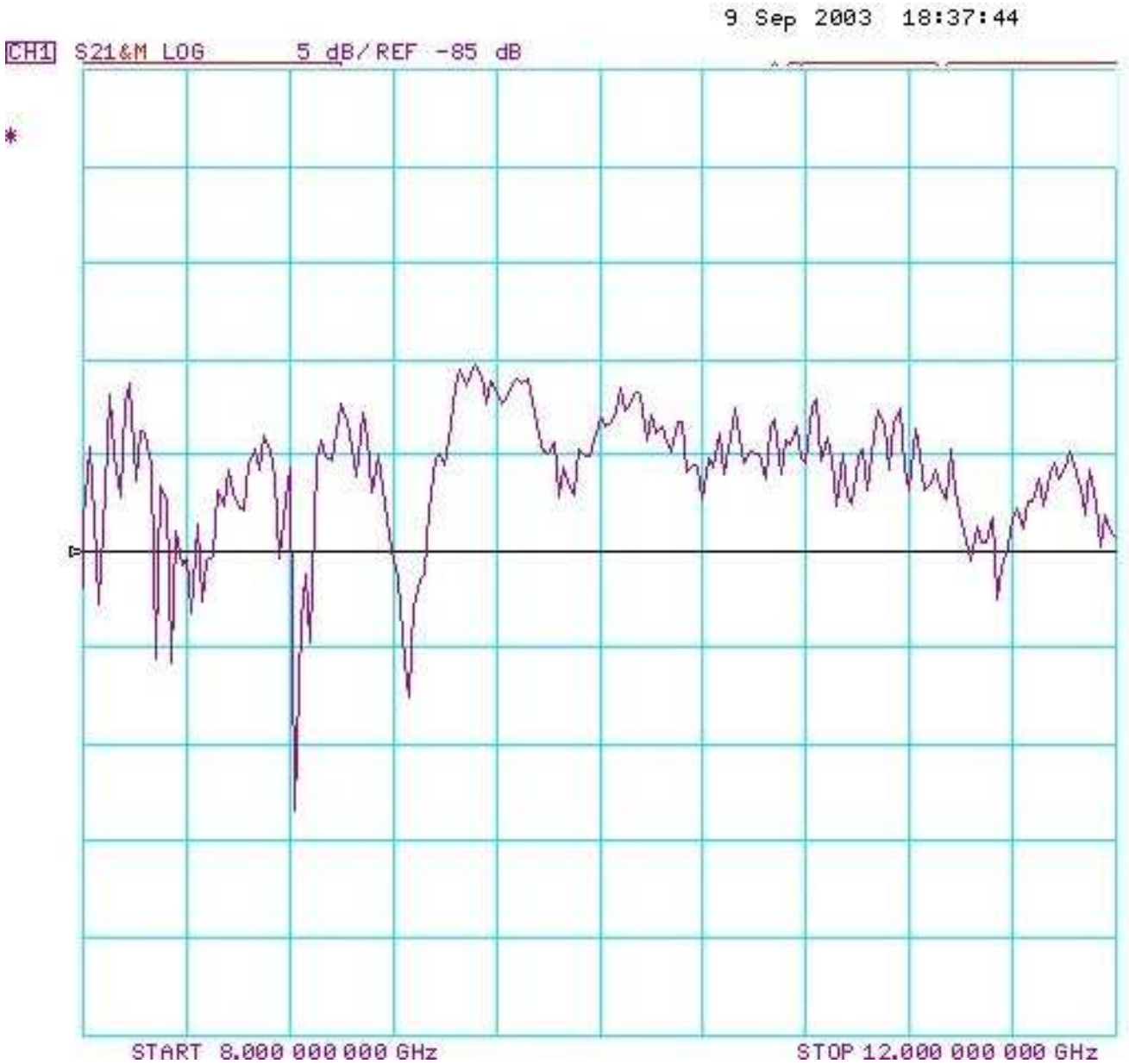

Figure 4.2 Signal from Setup-I

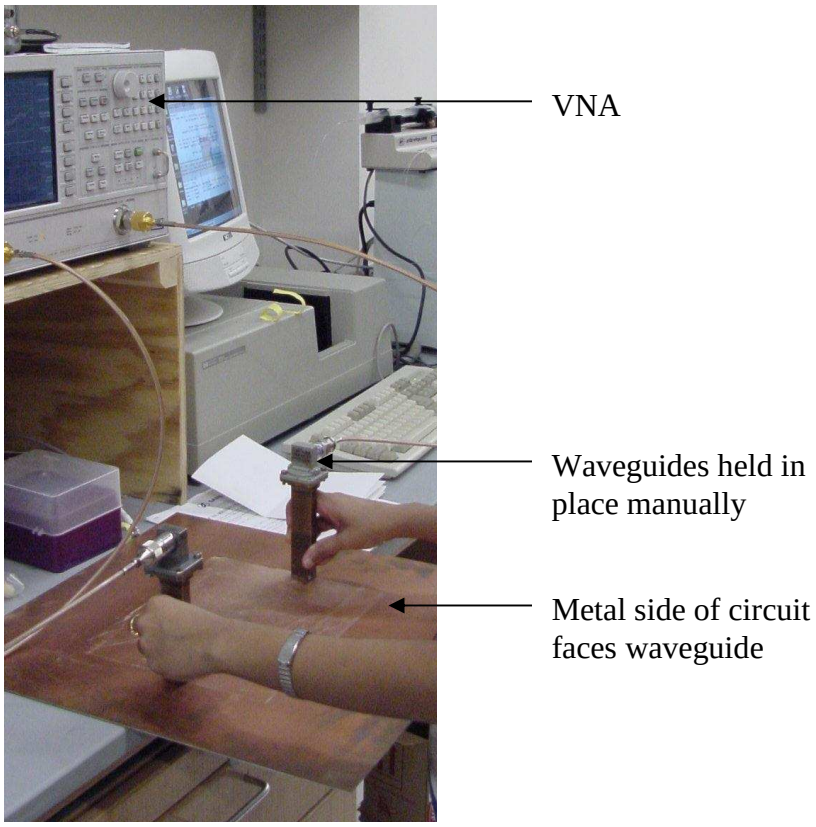

Figure 4.3 Setup-I.

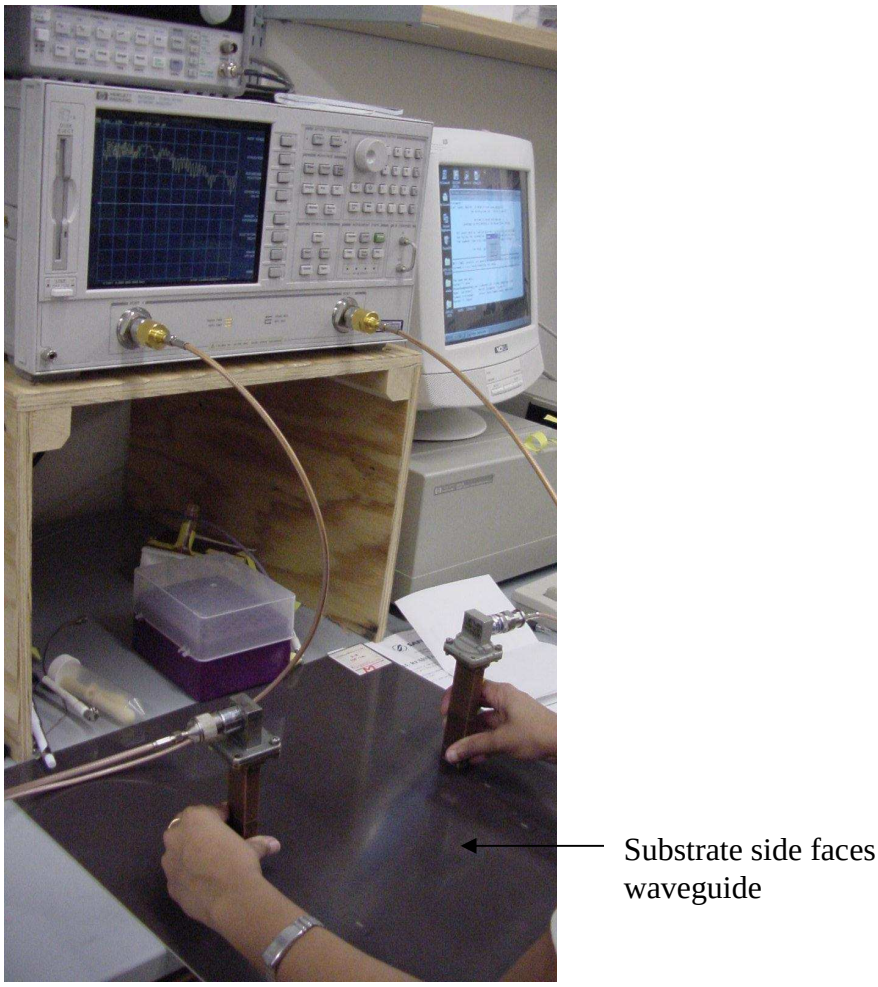

Figure 4.4 Setup-II with waveguide feeding slots from substrate side.

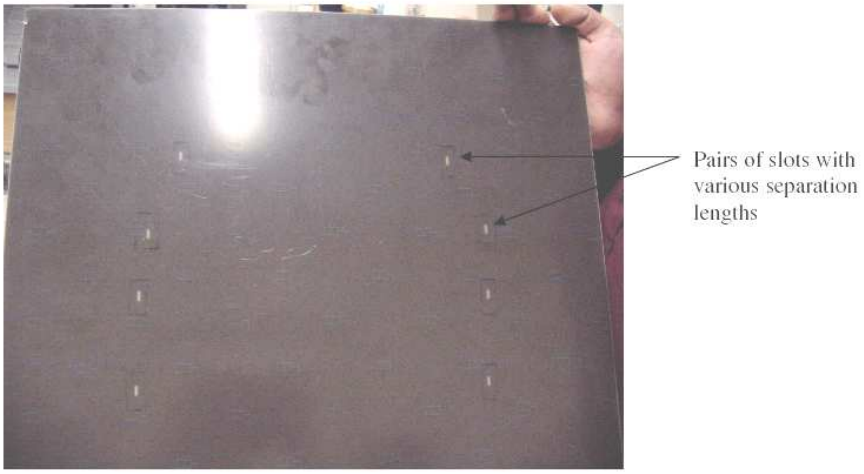

Figure 4.5 Slots made on ground plane seen from substrate side.

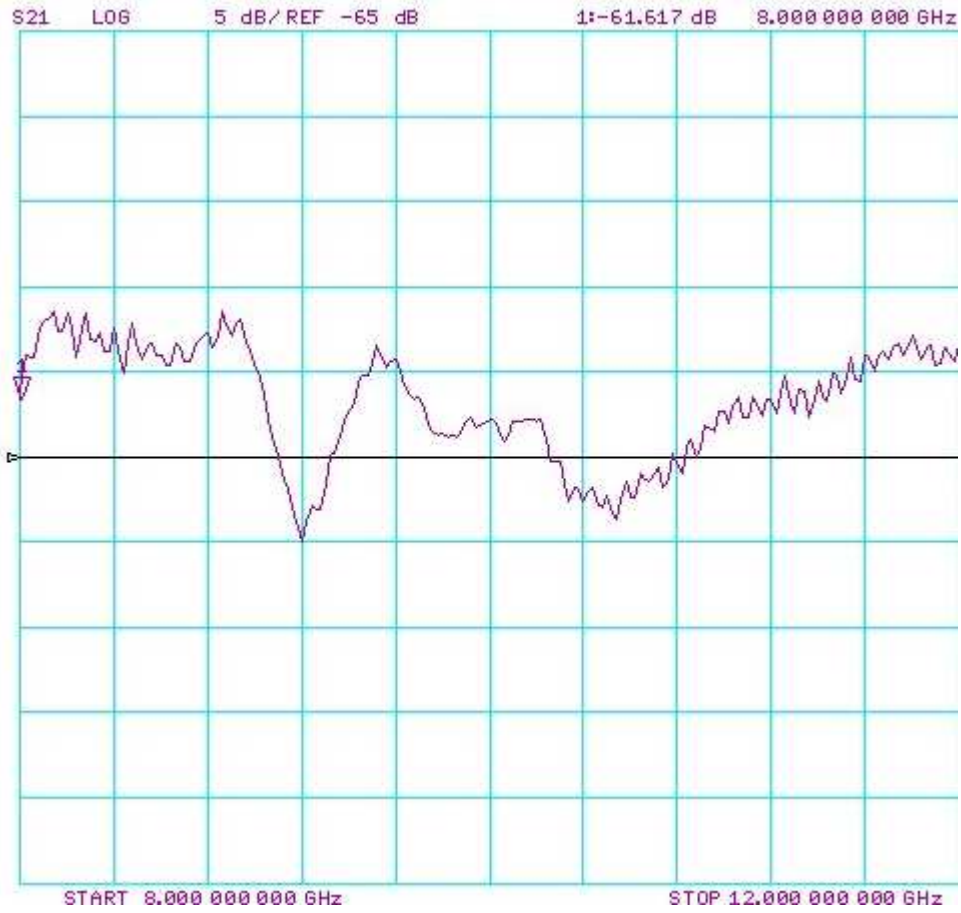

Figure 4.6 Signal from Setup-II.

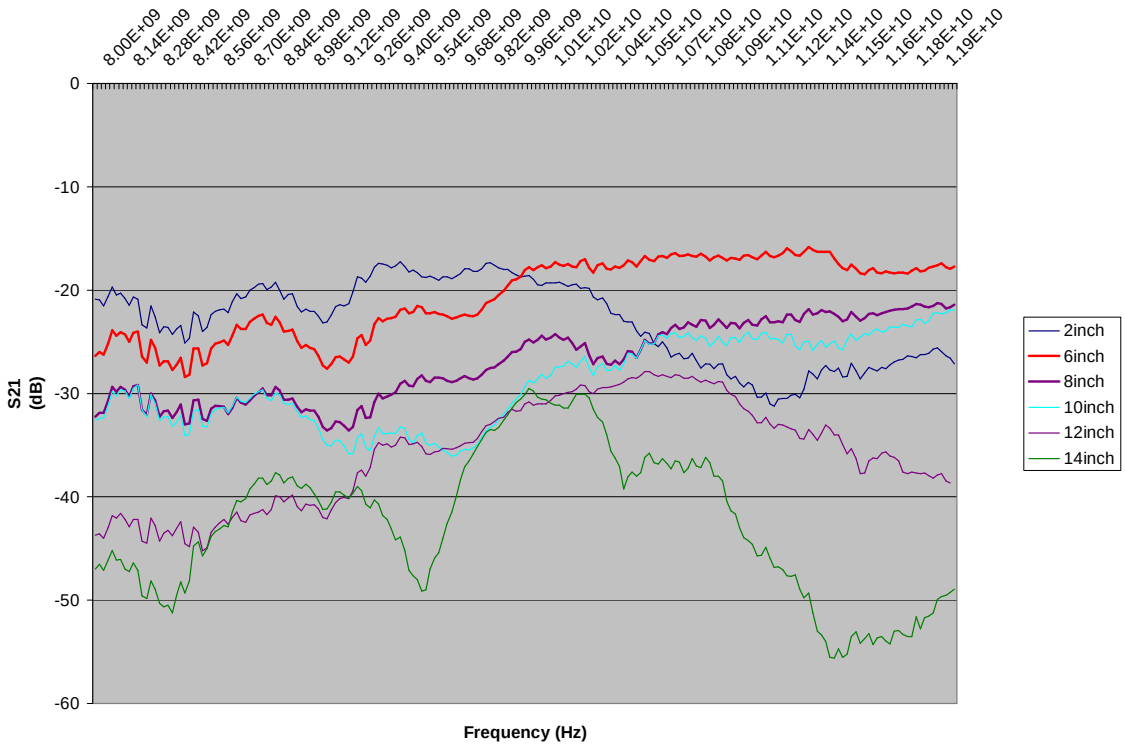

Figure 4.7 Raw data (includes all the transitions) from VNA showing decreasing transmission for increasing line lengths(Final Setup)

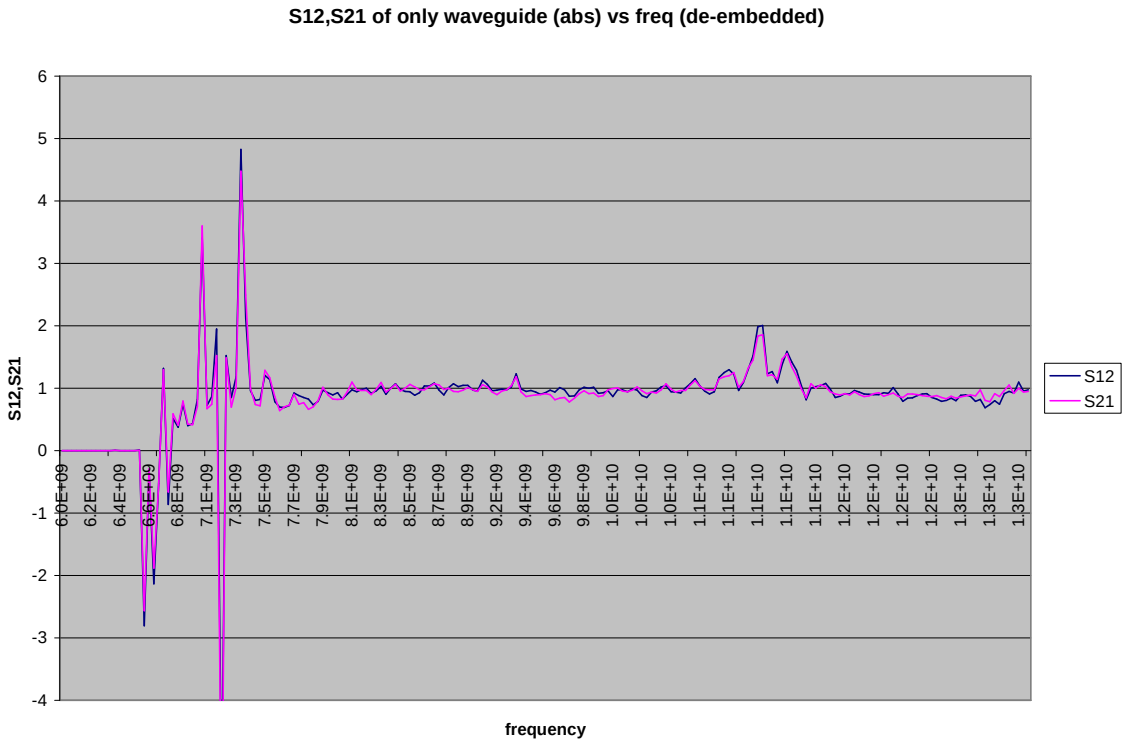

Figure 4.8 Waveguide de-embedded from coax and coax-to-waveguide transitions.

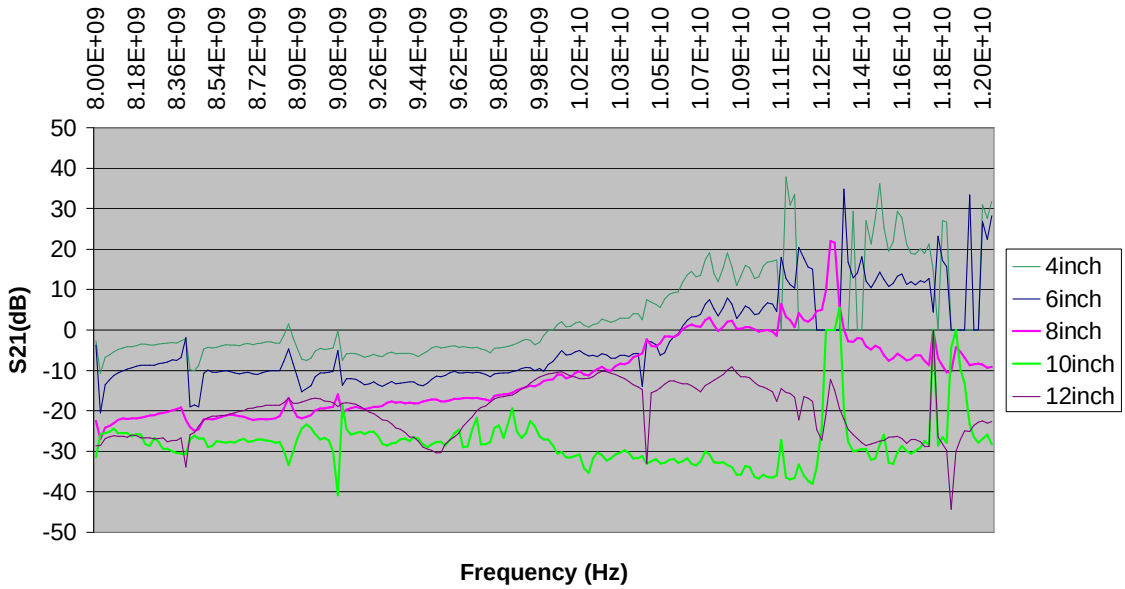

Figure 4.9 De-embedded data (transition effects removed) from the final setup showing the transmission parameters decreasing with increasing line lengths.

Chapter 5

Simulation Results

Simulations were carried out using HFSS. The setup was simulated from scratch.

1. X-Band Waveguide:

   The waveguide was first simulated to check for the design accuracy. The results obtained were as expected. Fig. 5.1 shows the S21 of the waveguide. The S21 was very low below the cutoff frequency of the waveguide. The transmission was almost 100% above the cutoff frequency.

2. Microstrip:

   A microstrip line was simulated with ports on each end of the line. FR_4 was used as the substrate. The S21 was again as expected. The line was simulated with a finite conductivity material and again with a perfect conductor. The plots (Fig. 5.2) for S21 show that the transmission is higher on a perfect conductor material when compared to the finite conductivity material.

3. Introducing Waveguides in the setup:

   Slots in their first resonance were then introduced with the previous setup. The waveguides were now used to feed the slots. Ports were setup on one end of the waveguides and the other end fed the slots from the substrate side. Fig. 5.3 shows the S21 obtained from the entire setup with the waveguides feeding the slots and the microstrip fed by the slots. The S21 was observed to drop by 30dB. This was justified because of the huge impedance mismatch between the slots and the microstrip line. The goal was to reduce the mismatch to favor the transmission between the two ports.

To achieve a better impedance match

- Line width and dielectric thickness were changed to provide a better match between the slot and the line (Table 5.1).
- Slot was designed to operate at the second resonance to reduce the impedance of the slot and provide a better match with the low impedance line. Also, a flared waveguide was used to provide a smooth transition and to reduce the relatively small mismatch between the waveguide and the slot.
- Slot width was also changed to sharpen the resonance.

5.1 Equivalent model of the setup

The entire setup with the pair of waveguides, slots, and the microstrip line can be modeled as in Fig. 5.4.
Z_{SRC1} and Z_{SRC2} are the Port Impedances in HFSS
Z_{WG1} and Z_{WG2} are the waveguide impedances
Z_{Slot1} and Z_{Slot2} are the Slot Impedances at their first resonance

Table 5.1 and table 5.2 compare the reflection and transmission parameters obtained by varying the line width and dielectric thickness using HFSS and the parameters derived from the model. The S11 and S21 in the model are calculated using both the waveguide-to-slot and slot-to-microstrip transitions. As seen from the model entries in the table, the reflection coefficient (S11) decreases as the line impedance increases. This trend is as expected because the line impedance gets closer to the slot impedance. The mismatch is still high and thus the high reflection coefficient. A similar trend is observed in the results obtained from simulations. With the dielectric thickness kept constant (1 mil) and by decreasing the line width the S11 is observed to decrease and the S21 increases. In the nest iteration, the dielctric thickness was increased while the line width was maintained at 20 mils. The trend observed was the same but the S11 and S21 didn't have a significant change when the dielctric

thickness was changed from 5 mils to 10 mils. Also, while comparing the results obtained from the 20 mil, 1 mil line and those obtained from the 2 mil, 1 mil and 20 mil, 10 mil lines, the 2 mil, 1 mil line had more transmission than the 20 mil, 10 mil line. This is because the line is lossy due to a finite conductivity material assignment.

To reduce the mismatch, the slot was designed to operate at it's second resonance. The impedance at it's second resonance approaches the microstrip impedance. Also, a flared waveguide was used. This reduces the impedance mismatch and thus improves the S11 drastically as seen from Table 5.2. Fig. 5.5 shows the trend between the simulations and the models.

					Simulation		*Model*	
Line W(mils)	Dielectric T(mils)	Line Z(ohm)	Slot Z(ohm)	W/G Z(ohm)	S11(dB)	S21(dB)	S11(dB)	S21(dB)
20	1	9.3	280	266	-2.42	-27.2	-0.58	-18
10	1	17	280	266	-4	-24.7	-1.05	-13.3
20	5	35	280	266	-4.18	-15.9	-2.18	-8
2	1	54	280	266	-6.55	-17.1	-3.39	-5.31
20	10	56	280	266	-4.33	-15.2	-3.52	-5.1

Table 5.1 S parameters obtained from simulations and the model for the slot operating at first resonance

					Simulation		*Model*	
Line W(mils)	Dielectric T(mils)	Line Z(ohm)	Slot Z(ohm)	W/G Z(ohm)	S11(dB)	S21(dB)	S11(dB)	S21(dB)
20	1	9.3	45	377	-10.7	-21.4	-7.83	-13.3
10	1	17	45	377	-13.4	-18.9	-11.1	-10.3
20	5	35	45	377	-15.65	-14.3	-22.25	-8.519
2	1	54	45	377	-16.8	-13.8	-25	-8.453
20	10	56	45	377	-15.78	-14.11	-23.45	-8.485

Table 5.2 S parameters obtained from simulations and the model for the slot operating at second resonance

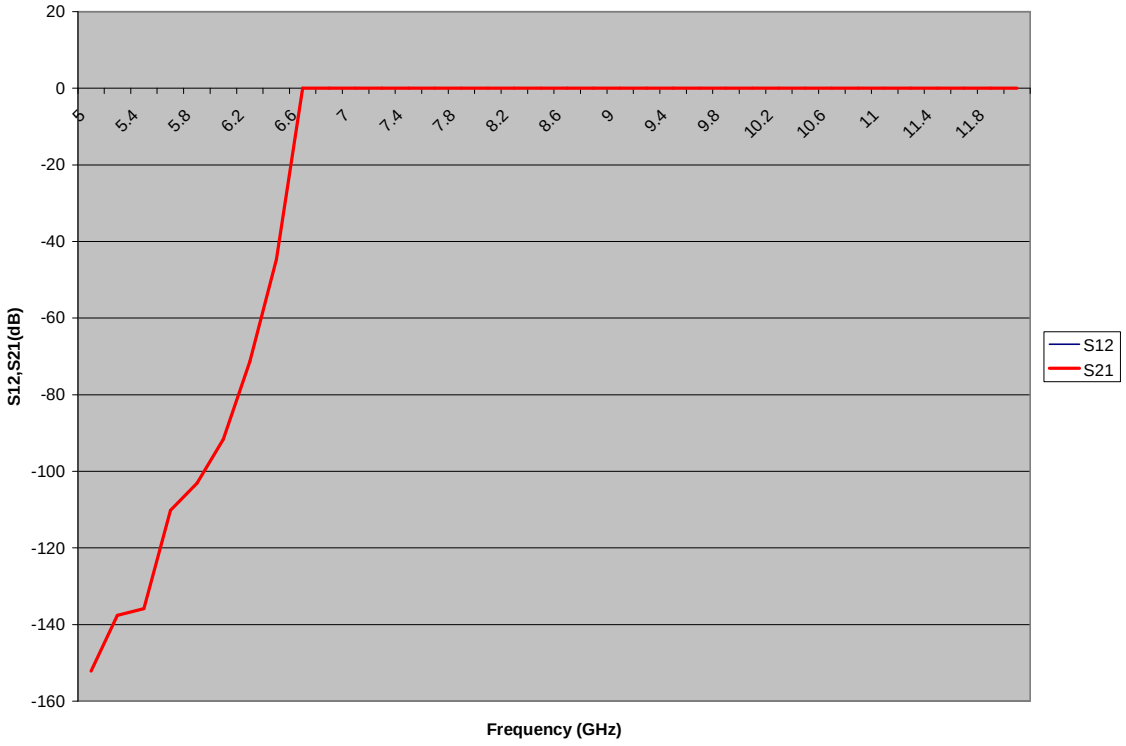

Figure 5.1 Transmission through a waveguide in HFSS

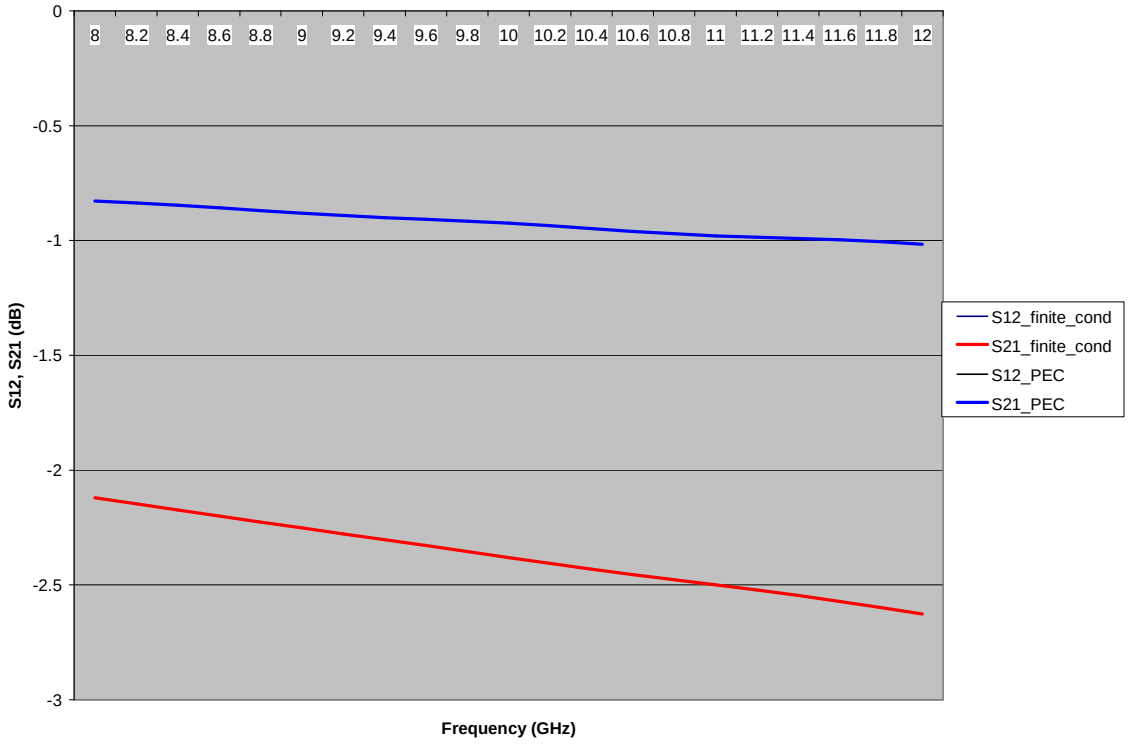

Figure 5.2 S21 for a perfect conductor microstrip and a finite conductivity microstrip

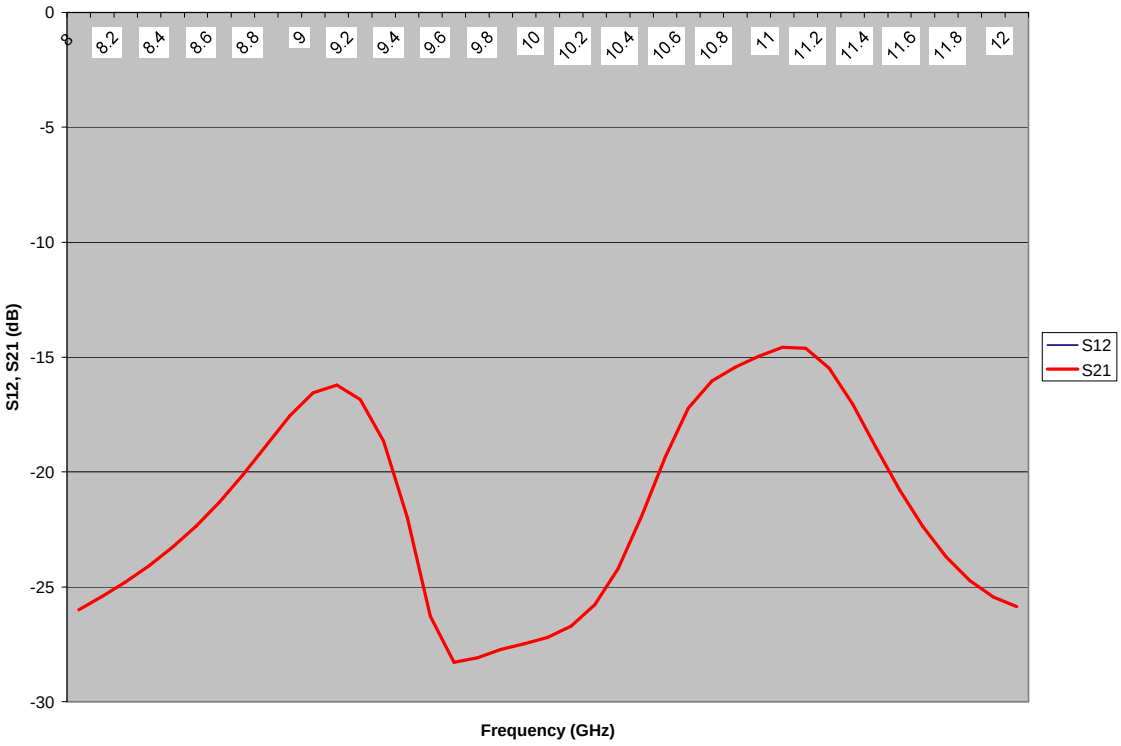

Figure 5.3 S21 through the setup with ports on end of each waveguide feeding slots

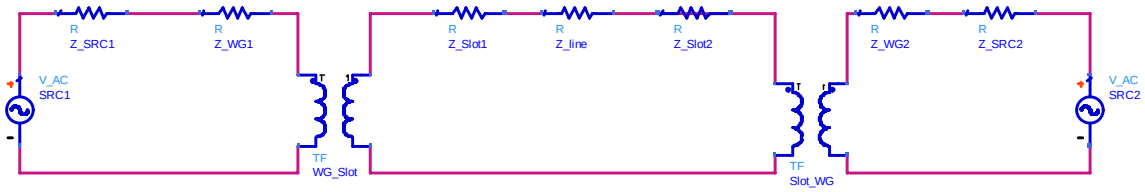

Figure 5.4 Equivalent circuit model

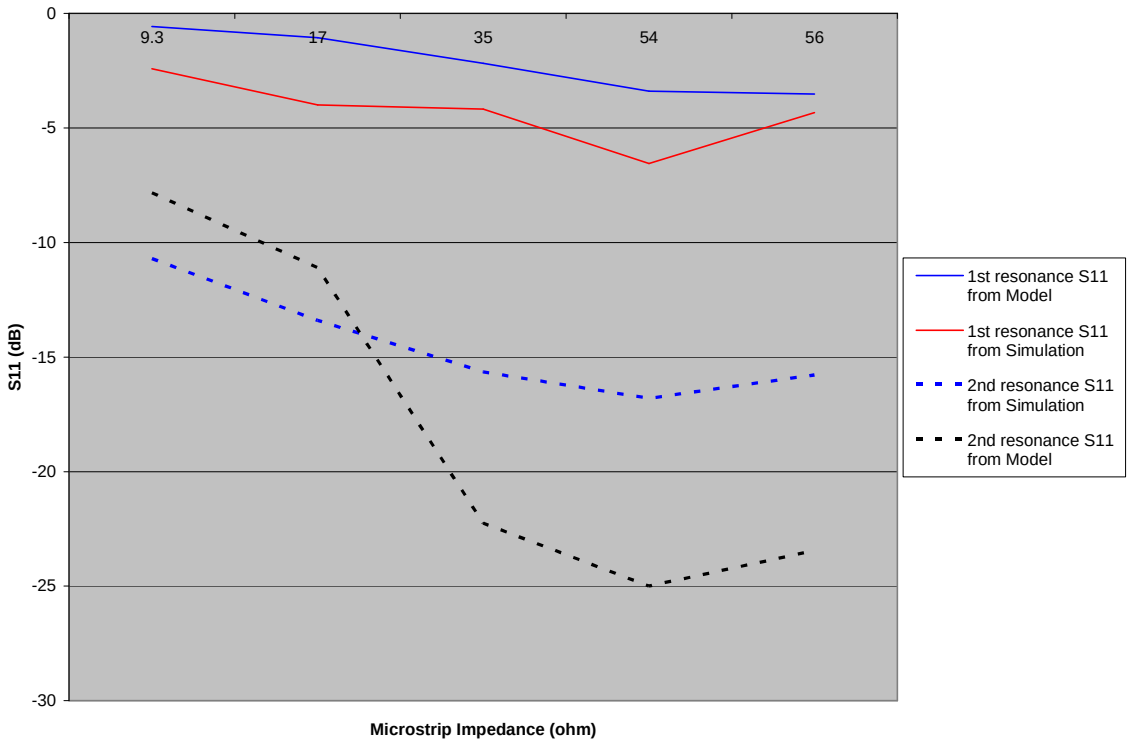

Figure 5.5 Comparison of S11 between model and simulation for 1st and 2nd resonance of the slot

Chapter 6

Conclusions and Future Work

This thesis detailed the various aspects of losses in slot-coupled microstrip transmission lines fed by waveguides. The goal was to increase the transmission in microstrip lines by reducing the mismatch between the various transitions from the waveguide and the microstrip lines. Experiments were carried out with different lengths of microstrip transmission lines fed by slots in the ground plane. Different methods to reduce the mismatch were used. Step-by-step experimental setup was described and the reasons for the failure of the initial setup's were described too. Extensive simulations also were carried out using HFSS to understand the low transmission found in the experiments. The HFSS simulations have agreed with the experimental results. The width of the transmission line, thickness of the dielectric were varied to improve the impedance match. Flared rectangular waveguides were also simulated. The slots were simulated for their first as well as second resonance. They provide a better match with the second resonance and the flared waveguides together lowering the reflections.

The experiments and simulations showed that the transmission was not too good because of the inherent mismatches in the circuit. The continuation of this work could be to implement stub matching to improve the impedance match between the microstrip and the slot. Also, flared waveguides feeding slots designed for the second resonance can provide a better impedance match with the microstrip line. Dielectric substrates [11] and dielectric lenses [4] could be used to reduce the reflection.

Bibliography

[1] Booker, H. [1946], 'Slot aerials and their relation to complementary wire aerials', *Journal of Institute of Electrical Engineers* pp. 620–626.

[2] Burberry, R. [1992], *VHF and UHF Antennas*, Peter Peregrinus Ltd.

[3] *De-embedding and Embedding S-Parameter Networks Using a Vector Network Analyzer* [2001]. Agilent Application Note 1364-1.

[4] Filipovic, D. and Gearhart, S. [1993], 'Double-slot antennas on extended hemispherical and elliptical silicon dielectric lenses', *IEEE Transactions on microwave theory and techniques* **41**(10).

[5] Ho, T. and Shih, Y. [1989], 'Spectral-domain analysis of e-plane waveguide to microstrip transitions', *IEEE Transactions on Microwave Theory Tech.* **37**.

[6] Ida, N. [2004], *Engineering Electromagnetics*, Springer-Verlag.

[7] Kaneda, N., Yongxi, Q. and Itoh, T. [1999], A broadband microstrip-to-waveguide transition using quasi-yagi antenna, *in* 'Microwave Symposium Digest, 1999 IEEE MTT-S International', pp. 1431–1434.

[8] Kerr, A. [1999], Surface impedance of superconductors and normal conductors in em simulators, Technical report, MMA Memo No. 245, National Radio Astronomy Observatory, Charlottesville, VA.

[9] Kooi, J., Chattopadhyay, G., Withington, S., Rice, F., Zmuidzinas, J., Walker, C. and Yassin, G. [2003], 'A full-height waveguide to thin-film microstrip transition with

exceptional rf bandwidth and coupling efficiency', *International Journal of Infrared and Millimeter Waves* **24**(3).

[10] Menzel, W. and Klaassen, A. [1989], On the transition from ridged waveguide to microstrip, *in* '19th European Microwave Conference Proceedings', pp. 1265–1269.

[11] Rogers, R. and Neikirk, D. [1989], 'Radiation properties of slot and dipole elements on layered substrates', *International Journal of Infrared and Millimeter Waves* **10**(6), 697–728.

[12] Simon, W., Werthen, M. and Wolff, I. [1998], A novel coplanar transmission line to rectangular waveguide transition, *in* 'Microwave Symposium Digest, 1998 IEEE MTT-S International', pp. 257–260.

[13] Vayonakis, A., Luo, C., Leduc, H., Schoelkopf, R. and Zmuidzinas, J. [2002], The millimeter-wave properties of superconducting microstrip lines, *in* 'American Institute of Physics Conference Proceedings', pp. 539–542.

[14] Ward, J., Rice, F., Chattopadhyay, G. and Zmuidzinas, J. [1999], Supermix: A flexible software library for high-frequency circuit simulation, including sis mixers and superconducting elements, *in* 'Proceedings, Tenth International Symposium on Space Terahertz Technology', pp. 268–281.

APPENDIX
Code for simulation of superconducting microstrip in SuperMix

SuperMix is a software library written to aid in the calculation and optimization of the signal and noise performance of high-frequency circuits, especially those including superconductors and superconducting tunnel junctions [14].

```
#include "supermix.h"
main()
{
device::T = 4.2*Kelvin ; // Default temperature
device::Z0 = 50.*Ohm ; // Normalization impedance
// Define metal film
super_film nb1;
// Standard parameters for Niobium
nb1.Vgap = 2.9*mVolt ;
nb1.Tc = 9.2*Kelvin ;
double cm = 1.e4 * Micron;
nb1.rho_normal = 5.*Micro*Ohm*cm ;
// Set thickness
nb1.Thick = 2000.*Angstrom ;
// Define dielectrics
const_diel sio ;
const_diel vacuum ;
```

```
vacuum.eps = 1.0 ;
vacuum.tand = 0.0 ;
sio.eps = 5.6 ; // dielectric constant
sio.tand = 0. ; // loss tangent
// Now make a microstrip line
microstrip ms1;
ms1.top_strip(nb1) ; // use Nb film for top strip
ms1.ground_plane(nb1) ; // same for ground plane
ms1.superstrate(vacuum) ; // nothing above
ms1.substrate(sio) ; // SiO insulator
ms1.sub_thick = 2000.*Angstrom ; // SiO thickness
ms1.length = 100.0*Micron ; // microstrip length
ms1.width = 5.0*Micron ; // microstrip width
// Print out S21 for this microstrip from 100 to 1000 GHz, step by 10 GHz.
for(double freq = 100. ; freq <= 1000.; freq += 10)
{
device::f = freq*GHz ;
complex S21 = ms1.S(2,1) ; // The S(2,1) function returns S21.
cout << freq << " "
<< zabs(S21) << " " // Print |S21|
<< arg(S21)/Degree << " " // and arg(S21)
<< endl ;
}
}
```

APPENDIX
Connectors

Coaxial connectors are often used to interface two units such as the antenna to a transmission line, a receiver or a transmitter. They are used where the coupling between two components is not *smooth*. A coaxial connector is comprised of an inner conductor, dielectric (physical support and a constant spacing between inner and outer conductor), outer conductor (shields against EMI) and a jacket (for physical protection). They are available in the audio, video, digital, RF and microwave industries, each designed for a specific purpose and application. Connectors come in different sizes and for different frequencies. The frequency range is limited by the excitation of the first propagating mode in the coaxial structure.

The characteristic impedance of a coaxial connector depends on the diameter of the outer and inner conductor. Proper impedance match is required to prevent VSWR mismatches. The insertion loss, power handling capability, mechanical dimensions and durability etc should be kept in mind while selecting a coax connector. SMA-3mm(Sub-Miniature A) coax connectors are most commonly used for microwave systems. Their frequency range is upto 18 GHz, but high performance varieties can be used to 26.5 GHz. They have higher reflection coefficients than other connectors available for use to 24 GHz because of the difficulty to anchor the dielectric (teflon) support. 1.0mm connectors have been launched which are designed to support transmission all the way to 110 GHz.

Misalignment of the male pin with respect to the female contacts (Fig. B.1) is a major cause of connector failure.

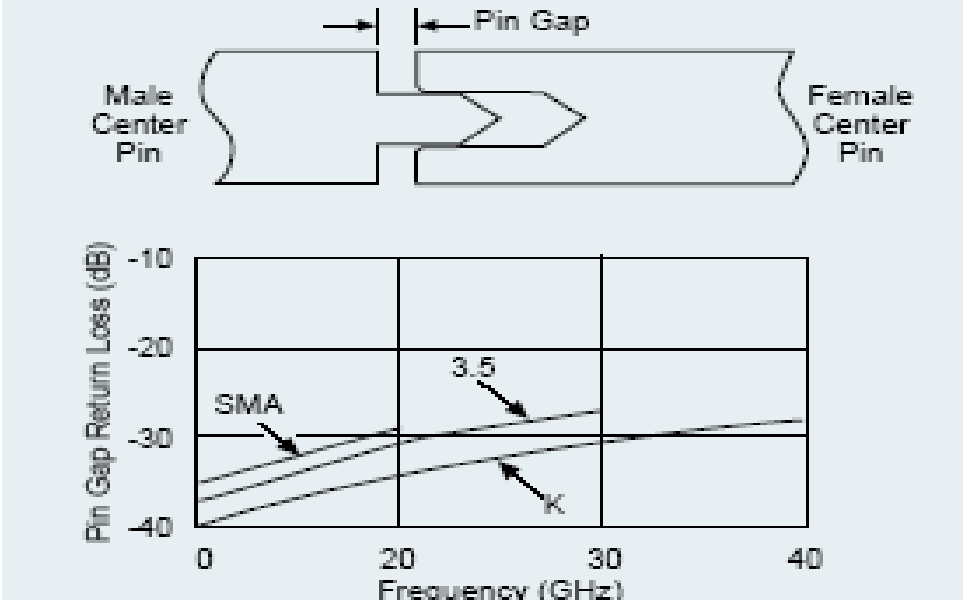

Figure B.1 Effect of pin gap dominant source of error in many connection systems

Inconspicuous damage to connectors gives rise to significant errors in measurements and thus proper care should be taken while handling connectors.

1. They should be regularly cleaned using solvents such as alcohol or a special-purpose cleaner.
2. The dielectric should not be brought into contact with the solvent.
3. When mating connectors align them properly to avoid bending or breaking the contact pins.
4. Rotate threaded sleeves to tighten and not the cable and other parts.
5. Do not Mate different types unless allowed to because the connection may not be mechanically stable and/or there may be significant impedance changes at the interface.
6. Do not touch the connector mating plane surfaces.
7. Examine for obvious defects: deformed threads or misaligned center conductor.
8. Use Torque Wrenches for connecting/disconnecting tiny connectors.